

Collision centrality and energy dependence of strange hadron production in Au + Au collisions at $\sqrt{s_{NN}} = 7.7\text{-}54.4$ GeV

Yan-ting Feng,¹ Zi-yao Song,¹ Feng-lan Shao,^{1,*} and Jun Song^{2,†}

¹*School of Physics and Physical Engineering, Qufu Normal University, Shandong 273165, China*

²*School of Physical Science and Intelligent Engineering, Jining University, Shandong 273155, China*

We apply an equal-velocity quark combination model to systematically study the transverse momentum (p_T) spectra of strange hadrons K_S^0 , ϕ , Λ , Ξ^- , Ω^- , $\bar{\Lambda}$, $\bar{\Xi}^+$ and $\bar{\Omega}^+$ at mid-rapidity in Au+Au collisions at $\sqrt{s_{NN}} = 7.7, 11.5, 19.6, 27, 39, 54.4$ GeV. Relative deviation between the model calculation and experimental data of these eight hadrons is generally about 2-3% at $\sqrt{s_{NN}} = 27, 39, 54.4$ GeV and in central collisions at 7.7, 11.5, 19.6 GeV. The deviation slightly increases up to about 4% in the semi-central and peripheral collision at $\sqrt{s_{NN}} = 7.7, 11.5, 19.6$ GeV. We systematically explain the dependence of two baryon-to-meson ratios $\bar{\Lambda}/K_S^0$ and Ω/ϕ on p_T , collision centrality and collision energy by the property of quark p_T spectra at hadronization. We derive the analytic relations between R_{CP} of hadrons and those of quarks, and we use them to naturally explain the species and p_T dependence of R_{CP} of those strange hadrons.

I. INTRODUCTION

Strange hadrons are excellent probes of high-energy collisions. The enhancement of strange hadrons was proposed as a signal of quark-gluon plasma (QGP) formation [1], and it was widely observed in relativistic heavy-ion collisions at SPS, RHIC and LHC [2–4]. In recent years, Beam Energy Scan (BES) experiments of STAR collaboration at RHIC have obtained rich experimental data of yield and transverse momentum (p_T) spectra of strange hadrons in Au+Au collisions at $\sqrt{s_{NN}} = 7.7\text{-}54.4$ GeV [5–9]. These experimental data contain valuable information on the property of hot nuclear matter and QCD phase transition at the finite baryon chemical potential, the mechanism of hadron production at hadronization, etc.

Existing theoretical studies on these newest data of strange hadrons at STAR are mainly of the global information on hadron freeze-out. Statistical model analysis on yield data of strange hadrons obtain the temperature and baryon chemical potential at the chemical freeze-out of hadrons [5, 10]. Analysis on p_T spectra data of strange hadrons provide the kinematic freeze-out temperature and collective radial flow at kinetic freeze-out of hadrons [5]. There also exist phenomenological extension by introducing Tsallis statistics at kinetic freeze-out to obtain a non-equilibrium parameter q besides the temperature and radial velocity [11–13].

On the other hand, the microscopic mechanism of strange hadrons production from the final-state parton systems created in heavy-ion collisions at STAR BES energies is also necessary to be studied in details. For example, we have known from the early heavy-ion collision experiments at RHIC [14–18] that the quark combination mechanism at hadronization is an effective mechanism to explain the hadron production in relativistic heavy-ion

collisions. How about the performance of this mechanism at STAR BES energies? The answer is not completely clear since the existing theoretical studies and comparison with the newest STAR data are relatively lack [19–21]. Further studies are necessary for deeply understanding the hadron production in heavy-ion collisions at STAR BES energies, which can also serve as the basis to better understand the hadron production in heavy-ion collisions at lower energies in fixed target experiments of STAR collaboration.

In this paper, we apply a quark combination model [20, 22, 23] to carry out a systematic study on p_T spectra of strange hadrons K_S^0 , ϕ , Λ , Ξ^- , Ω^- , $\bar{\Lambda}$, $\bar{\Xi}^+$ and $\bar{\Omega}^+$ at mid-rapidity in Au+Au collisions in different centralities at $\sqrt{s_{NN}} = 7.7, 11.5, 19.6, 27, 39, 54.4$ GeV. By a global fit to experimental data for p_T spectra of eight hadrons, we study the performance of equal-velocity combination (EVC) mechanism of constituent quark and antiquarks at hadronization, and we study the significance of the hadronization process imprinted in the final observation of strange hadrons. We also study two baryon-to-meson ratios $\bar{\Lambda}/K_S^0$ and Ω/ϕ as the function of p_T , where we focus on the self-consistent explanation on the collision centrality and energy dependence of two ratios by the properties of quark p_T distributions at hadronization. In study of the nuclear modification factor R_{CP} of strange hadrons, we drive several analytic relations between R_{CP} of hadrons and those of quarks, and we use them to naturally explain the species dependence of R_{CP} of different hadrons.

The paper is organized as follows. In Sec. II, we briefly introduce the model we used in this paper. In Sec. III, we show the global description of p_T spectra of strange hadrons in different centralities at $\sqrt{s_{NN}} = 7.7\text{-}54.4$ GeV. In Sec. IV, we discuss the centrality and collision energy dependence of baryon-to-meson ratios. In Sec. V, we study the nuclear modification factor of strange hadrons. The summary is given in Sec. VI.

* shaofl@mail.sdu.edu.cn

† songjun2011@jnxu.edu.cn

II. A QUARK COMBINATION MODEL WITH EVC

In this section, we briefly introduce a quark combination model used in this paper. The model was firstly proposed in [22] based on the finding of the quark number scaling property of hadronic p_T spectra in p Pb collisions at LHC energy. Subsequently, this scaling property was further found in pp and AA collisions at both RHIC and LHC energies and the model was systematically tested by the experimental data of hadronic p_T spectra and elliptic flow in those collisions [20, 23–28].

In the framework of quark combination mechanism, the inclusive momentum distribution of baryon (B_j) and meson (M_j) can be obtained by

$$f_{B_j}(p_B) = \int dp_1 dp_2 dp_3 f_{q_1 q_2 q_3}(p_1, p_2, p_3) \times \mathcal{R}_{B_j}(p_1, p_2, p_3; p_B), \quad (1)$$

$$f_{M_j}(p_M) = \int dp_1 dp_2 f_{q_1 \bar{q}_2}(p_1, p_2) \mathcal{R}_{M_j}(p_1, p_2; p_M). \quad (2)$$

Here, $f_{q_1 q_2 q_3}(p_1, p_2, p_3)$ is the joint momentum distribution function for q_1, q_2, q_3 and $f_{q_1 \bar{q}_2}(p_1, p_2)$ is that for q_1, \bar{q}_2 . $\mathcal{R}_{B_j}(p_1, p_2, p_3; p_B)$ denotes the probability density for a given $q_1 q_2 q_3$ with momenta p_1, p_2 and p_3 forming a baryon B_j with momentum p_B . $\mathcal{R}_{M_j}(p_1, p_2; p_M)$ denotes the probability density for a given $q_1 \bar{q}_2$ with momenta p_1 and p_2 forming a meson M_j with momentum p_M .

The hadronization is a non-perturbative process and the combination kernel functions \mathcal{R}_{B_j} and \mathcal{R}_{M_j} are hard to determine from the first principle calculation at the moment. Inspired by the quark number scaling property for hadronic p_T spectra at LHC [22, 26, 29], we can take the equal-velocity combination of constituent quarks and antiquarks as the main feature of hadron formation. In this case, we have

$$\mathcal{R}_{B_j}(p_1, p_2, p_3; p_B) = \kappa_{B_j} \prod_{i=1}^3 \delta(p_i - x_i p_B), \quad (3)$$

$$\mathcal{R}_{M_j}(p_1, p_2; p_M) = \kappa_{M_j} \prod_{i=1}^2 \delta(p_i - x_i p_M), \quad (4)$$

Momentum fraction x_i in baryon formula is $x_i = m_i/(m_1 + m_2 + m_3)$ and that in meson formula is $x_i = m_i/(m_1 + m_2)$. m_i is the constituent mass for quark of flavor i , and we take $m_s = 0.5$ GeV, $m_u = m_d = 0.3$ GeV. κ_{B_j} and κ_{M_j} are coefficients and independent of the momentum.

For the joint momentum distribution of quarks and antiquarks, we take the factorization approximation,

$$f_{q_1 q_2 q_3}(p_1, p_2, p_3) = f_{q_1}(p_1) f_{q_2}(p_2) f_{q_3}(p_3), \quad (5)$$

$$f_{q_1 \bar{q}_2}(p_1, p_2) = f_{q_1}(p_1) f_{\bar{q}_2}(p_2). \quad (6)$$

Substituting Eqs. (3)-(6) into Eqs. (1) and (2), we obtain

$$f_{B_j}(p_B) = \kappa_{B_j} f_{q_1}(x_1 p_B) f_{q_2}(x_2 p_B) f_{q_3}(x_3 p_B), \quad (7)$$

$$f_{M_j}(p_M) = \kappa_{M_j} f_{q_1}(x_1 p_M) f_{\bar{q}_2}(x_2 p_M). \quad (8)$$

We see that the momentum spectrum of hadron is simply the product of those of quarks at hadronization. This simple form yields some interesting flavor correlation among momentum distribution of different hadrons, e.g. those at p_T spectra [22, 26] and elliptic flows of different hadrons [30].

Coefficient κ_{B_j} and κ_{M_j} are independent of momentum but dependent on quark numbers. To determine them and clarify their physical meaning and importance, we write Eqs. (7) and (8) as

$$f_{B_j}(p_B) = N_{q_1 q_2 q_3} \kappa_{B_j} f_{q_1}^{(n)}(x_1 p_B) f_{q_2}^{(n)}(x_2 p_B) f_{q_3}^{(n)}(x_3 p_B), \quad (9)$$

$$f_{M_j}(p_M) = N_{q_1 \bar{q}_2} \kappa_{M_j} f_{q_1}^{(n)}(x_1 p_M) f_{\bar{q}_2}^{(n)}(x_2 p_M), \quad (10)$$

by introducing the normalized quark distribution $f_{q_i}^{(n)}(p) = N_{q_i} f_{q_i}(p)$. At the same time, we write hadron distribution as

$$f_{B_j}(p_B) = N_{B_j} f_{B_j}^{(n)}(p_B), \quad (11)$$

$$f_{M_j}(p_M) = N_{M_j} f_{M_j}^{(n)}(p_M). \quad (12)$$

Comparing Eqs. (9-10) and (11-12), we obtain

$$N_{B_j} = N_{q_1} N_{q_2} N_{q_3} \frac{\kappa_{B_j}}{A_{B_j}}, \quad (13)$$

$$N_{M_j} = N_{q_1} N_{\bar{q}_2} \frac{\kappa_{M_j}}{A_{M_j}}, \quad (14)$$

where

$$A_{B_j}^{-1} = \int f_{q_1}^{(n)}(x_1 p_B) f_{q_2}^{(n)}(x_2 p_B) f_{q_3}^{(n)}(x_3 p_B) dp_B, \quad (15)$$

$$A_{M_j}^{-1} = \int f_{q_1}^{(n)}(x_1 p_M) f_{\bar{q}_2}^{(n)}(x_2 p_M) dp_M. \quad (16)$$

Clearly, κ_{B_j}/A_{B_j} in Eq. (13) serves as the momentum-integrated probability of $q_1q_2q_3$ forming a baryon B_j . κ_{M_j}/A_{M_j} in Eq. (14) denotes that of $q_1\bar{q}_2$ forming a meson M_j . Supposing that quark system doubles in size, i.e., N_{q_i} doubles, then after hadronization N_h should also double. However $N_{q_1}N_{q_2}N_{q_3}$ in Eq. (13) increases 8 times and $N_{q_1}N_{\bar{q}_2}$ in Eq. (14) increases 4 times. Therefore, probability κ_{B_j}/A_{B_j} in Eq. (13) and κ_{M_j}/A_{M_j} in Eq. (14) should also play the role of the re-normalization to guarantee the unitarity of the hadronization. Following this argument, we can parameterize them as

$$\kappa_{B_j}/A_{B_j} \equiv P_{q_1q_2q_3 \rightarrow B_j} = C_{B_j} N_{iter} \frac{\overline{N}_B}{N_{qqq}}, \quad (17)$$

$$\kappa_{M_j}/A_{M_j} \equiv P_{q_1\bar{q}_2 \rightarrow M_j} = C_{M_j} \frac{\overline{N}_M}{N_q N_{\bar{q}}}. \quad (18)$$

Here, $N_{qqq} = N_q(N_q - 1)(N_q - 2) \approx N_q^3$ with $N_q = N_u + N_d + N_s$ in heavy-ion collisions is the combination number of all qqq . \overline{N}_B is the average number of all baryons. Then, \overline{N}_B/N_q^3 can denote the average probability of three quarks forming a baryon. The factor N_{iter} is the permutation number of $q_1q_2q_3$, and equals to 1, 3, 6 for $q_1q_2q_3$ with identical flavors, two identical flavors, and three different flavors, respectively. C_{B_j} is a refined parameter to account for the probability of forming different spin state at quark combination. The meson formula is similar. $\overline{N}_M/N_q N_{\bar{q}}$ denotes the average probability of a $q\bar{q}$ pair forming a meson. C_{M_j} account for the probability of forming the meson with given spin state.

In this paper, we only consider the production of ground state meson $J^P = 0^-, 1^-$ and baryon $J^P = (1/2)^+, (3/2)^+$ in flavor SU(3) group. We introduce a parameter $R_{D/O}$ to denote the relative probability of forming decuplet baryon to octet baryon with the same quark flavor, and introduce a parameter $R_{V/P}$ to denote the relative probability of vector meson to pseudo-scalar meson with same quark flavor. Then C_{B_j} and C_{M_j} can be written as

$$C_{B_j} = \begin{cases} \frac{1}{1+R_{D/O}} & \text{for } J^P = (1/2)^+ \\ \frac{R_{D/O}}{1+R_{D/O}} & \text{for } J^P = (3/2)^+ \end{cases}, \quad (19)$$

except $C_\Lambda = C_{\Sigma^0} = 1/(2 + R_{D/O})$, $C_{\Sigma^{*0}} = R_{D/O}/(2 + R_{D/O})$, $C_{\Delta^{++}} = C_{\Delta^-} = C_{\Omega^-} = 1$, and

$$C_{M_j} = \begin{cases} \frac{1}{1+R_{V/P}} & \text{for } J^P = 0^- \\ \frac{R_{V/P}}{1+R_{V/P}} & \text{for } J^P = 1^- \end{cases}. \quad (20)$$

Here, we take $R_{V/P} = 0.55 \pm 0.05$ to reproduce the experimental data of yield ratios K^*/K and ϕ/K in high energy pp and pPb collisions [31, 32]. We take $R_{D/O} = 0.5 \pm 0.04$ by fitting the experimental data of yield ratios Ξ^*/Ξ and Σ^*/Λ in high-energy pp collisions [33].

For global production of baryons and mesons, i.e., \overline{N}_B and \overline{N}_M , we have obtained their empirical solution [34],

$$\overline{N}_M = \frac{x}{2} \left[1 - z \frac{(1+z)^a + (1-z)^a}{(1+z)^a - (1-z)^a} \right], \quad (21)$$

$$\overline{N}_B = \frac{xz}{3} \frac{(1+z)^a}{(1+z)^a - (1-z)^a}, \quad (22)$$

$$\overline{N}_{\bar{B}} = \frac{xz}{3} \frac{(1-z)^a}{(1+z)^a - (1-z)^a}, \quad (23)$$

where $x = N_q + N_{\bar{q}}$ and $z = (N_q - N_{\bar{q}})/x$. $a = 1 + (\overline{N}_M/\overline{N}_B)_{z=0}/3$ characterizes the production competition of baryon to meson at $z = 0$ and is tuned to be $a \approx 4.86 \pm 0.1$ in relativistic heavy-ion collisions [35].

When quark distributions $f_{q_i}(p)$ are given, momentum distributions of hadrons $f_h(p)$ and their integrated yields N_h can be directly calculated using the model. In order to compare with experimental data, the decay contribution of short-life resonance should be also considered,

$$f_{h_j}^{(final)}(p) = f_{h_i}(p) + \sum_{i \neq j} \int dp' f_{h_i}(p') D_{ij}(p', p). \quad (24)$$

The decay function $D_{ij}(p', p)$ is determined by the decay kinematics and decay branch ratios [36].

III. TRANSVERSE MOMENTUM SPECTRUM OF STRANGE HADRONS

In this section, we use the above EVC model to calculate p_T spectra of strange hadrons at mid-rapidity in Au + Au collisions at $\sqrt{s_{NN}} = 7.7, 11.5, 19.6, 27, 39$ and 54.4 GeV, and make systematic comparison with the experimental data [7–9, 37, 38]. First, we reduce the formulas in the model to those in one-dimensional p_T space at mid-rapidity $y = 0$. The momentum distribution function $f(p)$ reduces to $f(p_T) \equiv dN/dp_T$ and momentum integration in Eqs. (15) and (16) reduce to p_T integration.

The model needs p_T spectra of quarks and antiquarks at hadronization $f_q(p_T)$ as the input, which are difficult to obtain from first principle calculations. Here, we take the following parametrization form for the normalized quark p_T spectrum

$$f_q^{(n)}(p_T) = \mathcal{N}_q (p_T + a_q)^{b_q} \left(1 + \frac{\sqrt{p_T^2 + m_q^2} - m_q}{n_q c_q} \right)^{-n_q}, \quad (25)$$

where \mathcal{N}_q is a normalized constant to assure $\int f_q^{(n)}(p_T) dp_T = 1$. Parameters a_q, b_q, n_q, m_q, c_q control the shape of the spectrum. We also need the numbers of quarks and antiquarks N_{q_i} so that $f_{q_i}(p_T) = N_{q_i} f_{q_i}^{(n)}(p_T)$ can be used to calculate p_T spectra of hadrons in our model.

For hadron production at mid-rapidity at the studied collision energies, we take the approximate isospin symmetry between up and down quarks, i.e., $f_u(p_T) = f_d(p_T)$ and $f_{\bar{u}}(p_T) = f_{\bar{d}}(p_T)$. We also assume the strangeness neutrality $f_s(p_T) = f_{\bar{s}}(p_T)$ according to our previous work [20]. Finally, we need three inputs $f_u(p_T)$, $f_{\bar{u}}(p_T)$ and $f_s(p_T)$ to calculate p_T spectra of light-flavor hadrons. They are fixed by fitting experimental data of identified hadrons in our model. Specifically, experimental data of p_T spectrum of ϕ are used to fix $f_s(p_T)$, i.e., quark number N_s and spectra parameters a_s , b_s , c_s , m_s and n_s . Because experimental data for p_T spectra of proton and antiproton are available only at $p_T < 2$ GeV/c [39], they can only constrain p_T spectra of up quarks in a narrow range ($p_{T,u} \lesssim 0.8$ GeV/c) and therefore we alternatively use experimental data for p_T spectra of Λ and $\bar{\Lambda}$ which cover a wider p_T range to fix $f_u(p_T)$ and $f_{\bar{u}}(p_T)$, respectively. Results for quark p_T spectra at mid-rapidity in Au+Au collisions in different centralities at $\sqrt{s_{NN}} = 7.7, 11.5, 19.6, 27, 39, 54.4$ GeV are shown in Figs. 1-3. Their properties are discussed latter in studying the baryon-to-meson ratios in Sec. IV and nuclear modification factors of hadrons in Sec. V.

Figs. 4-11 show model results for p_T spectra of different strange hadrons and their comparison with experimental data [7, 8, 37, 38]. Besides three hadrons ϕ , Λ , $\bar{\Lambda}$ which are used to constrain quark p_T spectra, results of other hadrons Ξ^- , $\bar{\Xi}^+$, Ω^- , $\bar{\Omega}^+$ as well as K_S^0 ¹ are shown as theoretical prediction. In addition, we also calculate p_T spectra of proton and antiproton and find they are in good agreement with the available data at $p_T < 2$ GeV/c, which are not shown here since we focus on strange hadrons in this paper. The systematic comparison between model results of eight strange hadrons and their experimental data can effectively test our model.

Considering that the p_T coverage and statistical uncertainties of experiment data of these hadrons are different in different centralities and/or at different collision energies, here in stead of the standard χ^2/ndf evaluation, we use the relative deviation

$$\bar{D} = \frac{1}{N_{data}} \sum_i^{N_{data}} \left| \frac{y_i^{(model)} - y_i^{(exp)}}{y_i^{(exp)}} \right| \quad (26)$$

¹ The p_T spectrum of K_S^0 is calculated as the equal weight mixing of that of K^0 and \bar{K}^0 . In addition, because kaon mass is smaller than the sum of constituent masses of down and strange quarks used in this paper, the direct combination of down and strange (anti-)quark is difficult to directly form the on-shell kaon. Therefore, we modify the kaon formation in EVC mechanism as follows: The combination of up/down and strange quark has a large probability (p_1) to firstly form an intermediate resonance like $K^*(892)$ and then decays into the on-shell kaon and pion; it has a small probabilities (p_2) to directly from the on-shell kaon. Here, we take $p_1 = 3/4$ and $p_2 = 1/4$ so that $p_1 m_{K^*} + p_2 m_K \approx 0.8$ GeV approximately equals to $m_u + m_s$ and approximately satisfies energy conservation.

to quantify our model description. Here, $y_i^{(exp)}$ is the central value of experimental data. Index i runs over all datum points of eight hadrons presented in Figs. 4-11 in the given collision centrality and at the given collision energy. Results of \bar{D} are shown in Table. I.

We see that the relative deviation \bar{D} in the studied collision centralities and collision energy range is generally a few percentages. \bar{D} at $\sqrt{s_{NN}} = 19.6, 27, 39$ and 54.4 GeV is about 0.02 in all collision centralities. \bar{D} in semi-central and peripheral collisions at $\sqrt{s_{NN}} = 7.7$ and 11.5 GeV is about 0.03-0.04, which is larger than, to a certain extent, that in peripheral collisions at the two energies and those at higher collision energies.

The small values of \bar{D} indicate that experimental data of p_T spectra of these eight hadrons in Au+Au collisions at $\sqrt{s_{NN}} = 7.7-54.4$ GeV can be self-consistently described by our model. Such a global agreement therefore indicates the important role of EVC mechanism at hadron production in these collisions. In the following two sections, we further test our model by the baryon-to-meson ratios and nuclear modification factors of identified hadrons, which are more sensitive to hadron production mechanism in heavy-ion collisions.

IV. BARYON TO MESON RATIOS

Baryon-to-meson ratio is a sensitive physical quantity to check the hadronization mechanism. RHIC experiments at the early years had shown an enhancement of baryon-to-meson ratios at the intermediate p_T in heavy-ion collisions. This enhancement is difficultly understood in traditional fragmentation mechanism but can be naturally described in quark (re-)combination mechanism. In this section, we study $\bar{\Lambda}/K_S^0$ and Ω/ϕ ratios at/in different collision energies and/or centralities.

In Fig. 12, we show the results of $\bar{\Lambda}/K_S^0$ as the function of p_T in Au+Au collisions with different centralities at $\sqrt{s_{NN}} = 7.7 - 54.4$ GeV and compare them with experimental data [7, 37]. Experiment data of $\bar{\Lambda}/K_S^0$ ratio exhibit an obvious dependence on the collision energy and centrality. We see an obvious decrease of the ratio with the decrease of collision energy. From central collisions to peripheral collisions, we also see the decrease of the ratio. The decrease magnitude of $\bar{\Lambda}/K_S^0$ with collision centrality is generally slower than that with collision energy. For experimental data of the central and semi-central collisions which have rich data points and cover broad p_T range, we always see a non-monotonic p_T dependence of the $\bar{\Lambda}/K_S^0$ ratio. The solid lines are our model results. They are generally in good agreement with experimental data. In the following text, we explain the underlying physics for the p_T , collision energy and centrality dependence of the ratio.

Firstly, we explain the non-monotonic p_T dependence of the $\bar{\Lambda}/K_S^0$ ratio. We examine the property of quark p_T spectra shown in Figs. 1-3 which is parameterized in Eq. (25). In the range $p_{T,q} \lesssim 1$ GeV/c (i.e., at low p_T for

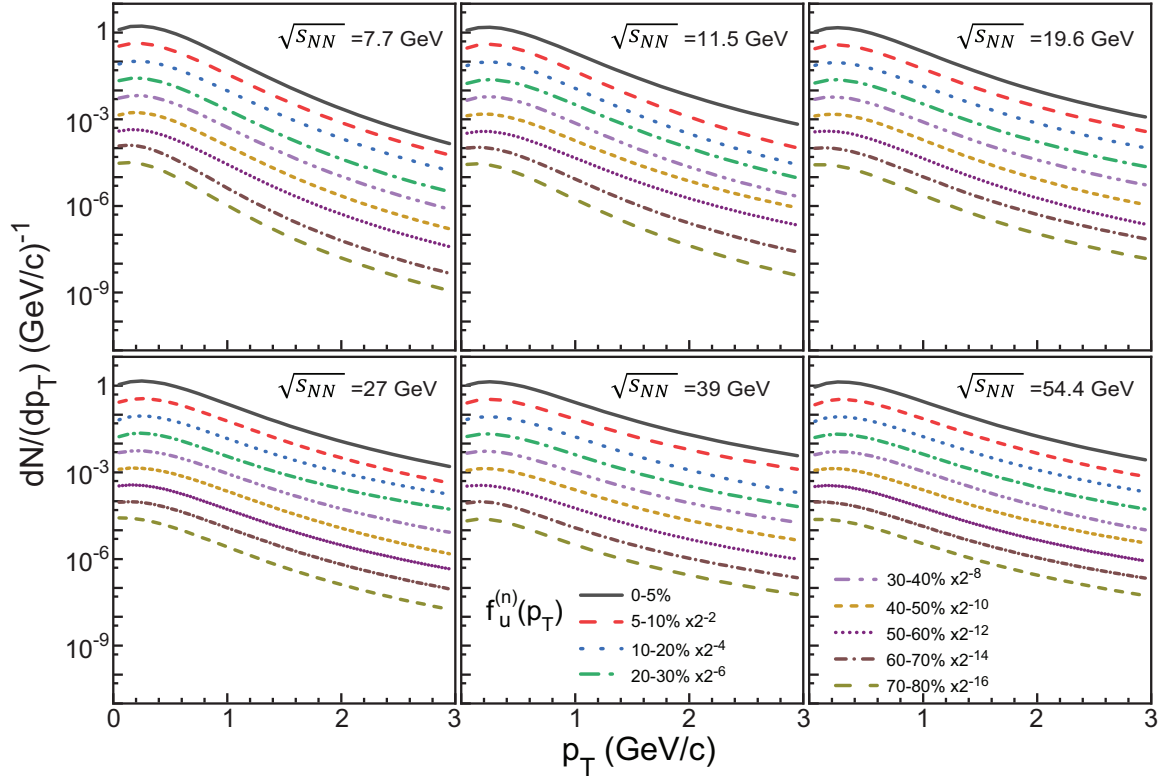


Figure 1. The p_T spectra of u quark in different centrality in Au + Au collisions at $\sqrt{s_{NN}}=7.7, 11.5, 19.6, 27, 39, 54.4$ GeV.

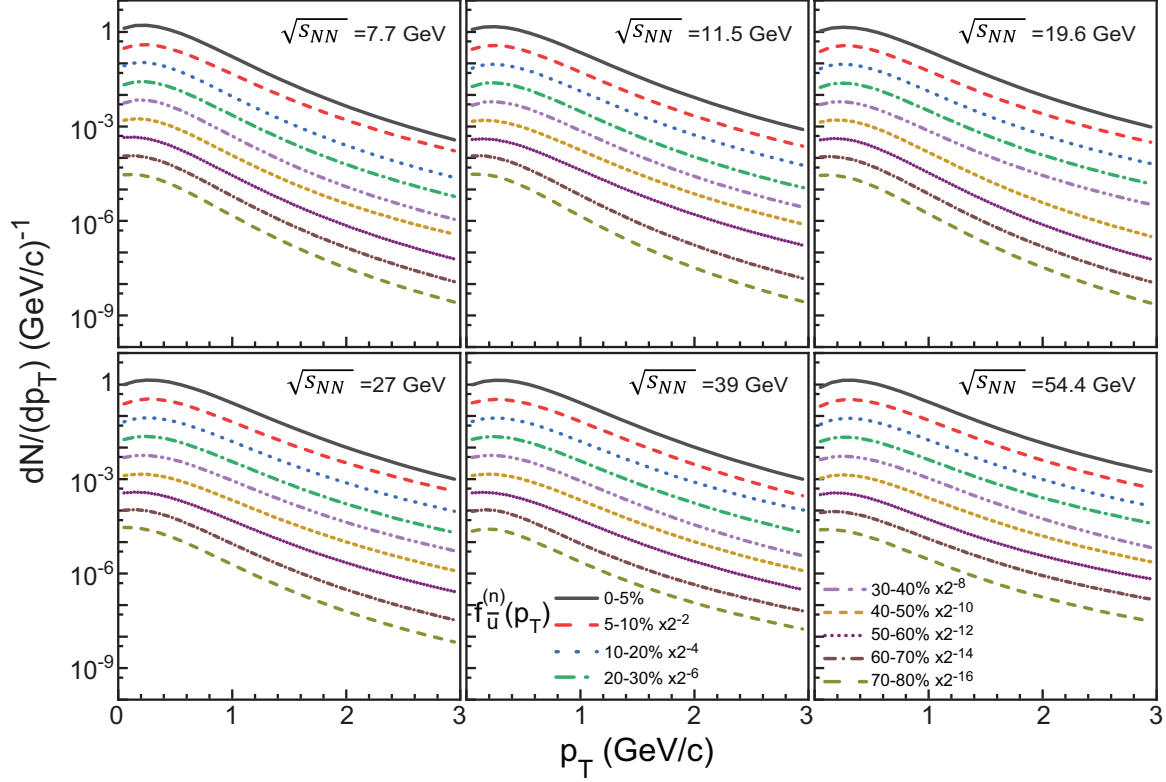


Figure 2. The same as 1 but for \bar{u} .

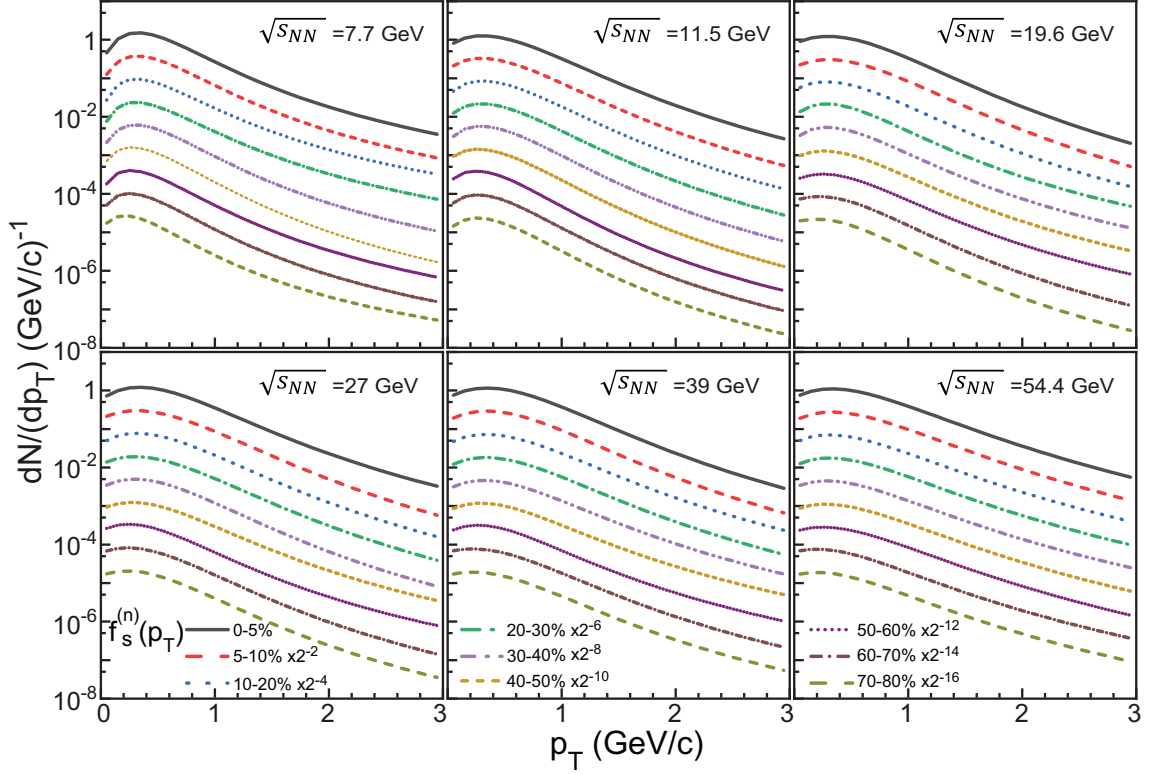


Figure 3. The same as 1 but for s .

Table I. Relative deviation of theory and experiment for various collision centralities and energy in Au+Au collisions at $\sqrt{s_{NN}} = 7.7-54.4$ GeV [7–9, 37, 38].

Centrality	7.7	11.5	19.6	27	39	54.4
0 – 5%	0.0279	0.0170	0.0189	0.0166	0.0167	0.0214
5 – 10%	0.0442	0.0341	0.0265	0.0308	0.0240	0.0243
10 – 20%	0.0263	0.0226	0.0129	0.0121	0.0167	0.0226
20 – 30%	0.0265	0.0286	0.0174	0.0138	0.0120	0.0305
30 – 40%	0.0236	0.0285	0.0197	0.0134	0.0193	0.0248
40 – 60%	0.0412	0.0325	0.0159	0.0224	0.0181	0.0241
60 – 80%	0.0436	0.0411	0.0256	0.0205	0.0209	0.0228

quarks), quark p_T spectrum behaves approximately as

$$dN_{q_i}/dp_T \propto p_T^{\alpha_i} \exp[-\sqrt{p_T^2 + m_i^2}/T_i], \quad (27)$$

where the exponent parameter $\alpha_i > 0$ and slop parameter $T_i > 0$. Then $\bar{\Lambda}/K_S^0$ ratio in the low p_T range ($p_T \approx$

$2 - 3p_{T,q} \lesssim 3$ GeV/c)

$$\begin{aligned} \frac{\bar{\Lambda}}{K_S^0} &= \frac{\kappa_\Lambda f_u(x_u p_T) f_d(x_d p_T) f_s(x_s p_T)}{\kappa_K f_s(x'_s p_T) f_{\bar{u}}(x'_u p_T)} \\ &= \text{coe} \times p_T^{\alpha_u} \\ &\times \exp \left[-\sqrt{x_u^2 p_T^2 + m_u^2} \left(\frac{2}{T_u} + \frac{m_s/m_u}{T_s} \right) \right] \\ &\times \exp \left[+\sqrt{x_u'^2 p_T^2 + m_u^2} \left(\frac{1}{T_{\bar{u}}} + \frac{m_s/m_u}{T_s} \right) \right], \end{aligned} \quad (28)$$

where we use $\alpha_u \approx \alpha_{\bar{u}}$ to simplify the expression. Because the exponential terms change weakly with p_T , the behavior of $\bar{\Lambda}/K_S^0$ ratio in the low p_T range is therefore

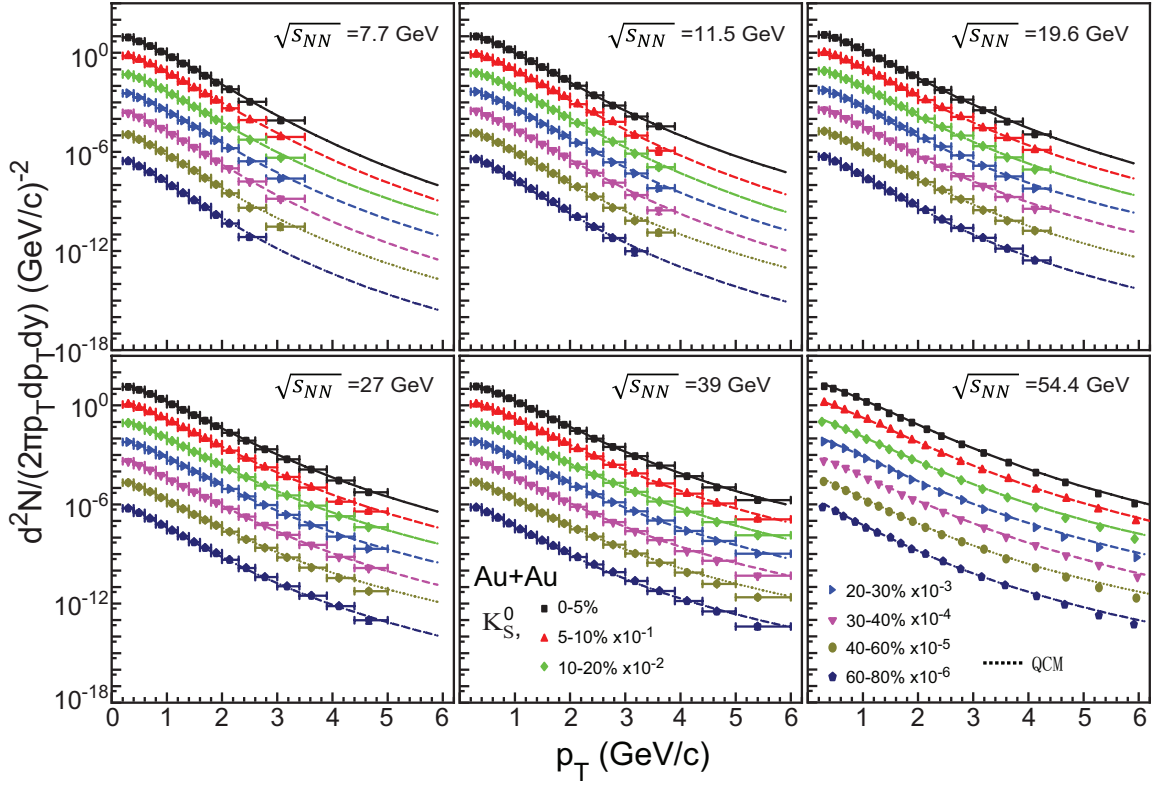


Figure 4. The p_T spectra of K_S^0 at mid-rapidity ($|y| < 0.5$) from Au + Au collisions at $\sqrt{s_{NN}}=7.7$ -54.4 GeV. Symbols are the experimental data [7, 8, 37] and lines are the results of our model. Spectra of some hadrons are scaled by factors 10 from central to peripheral collisions for clarity.

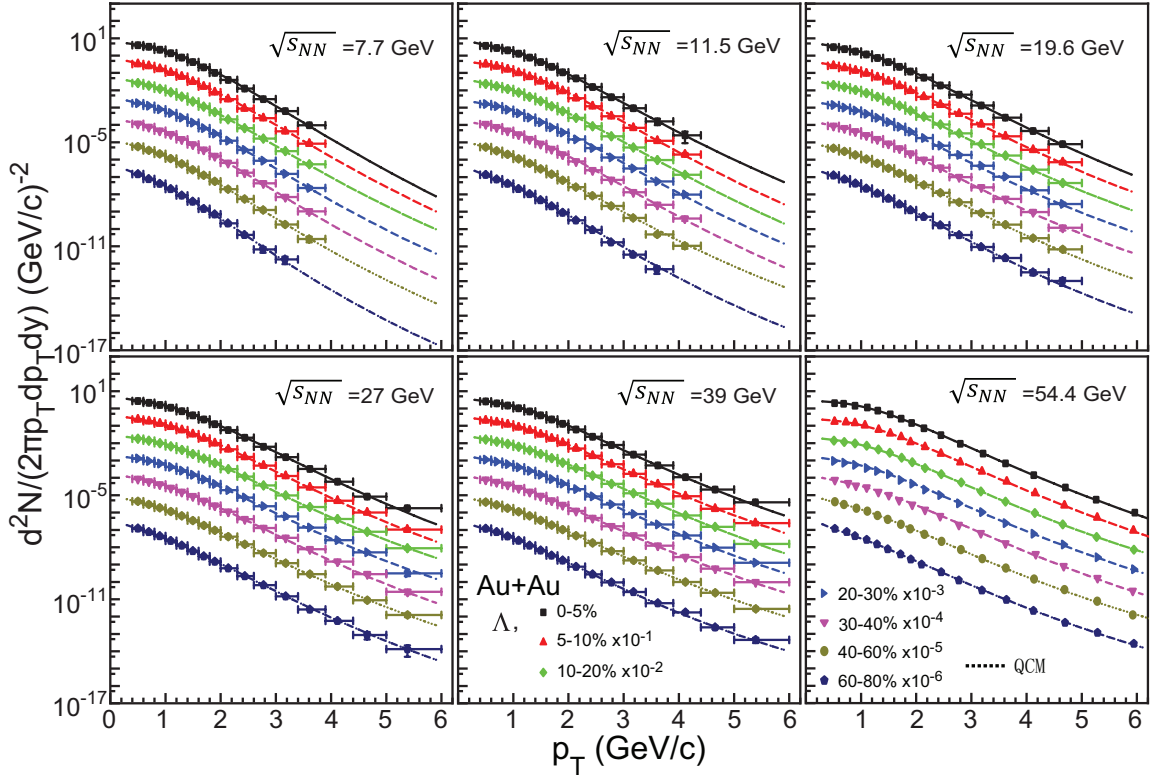
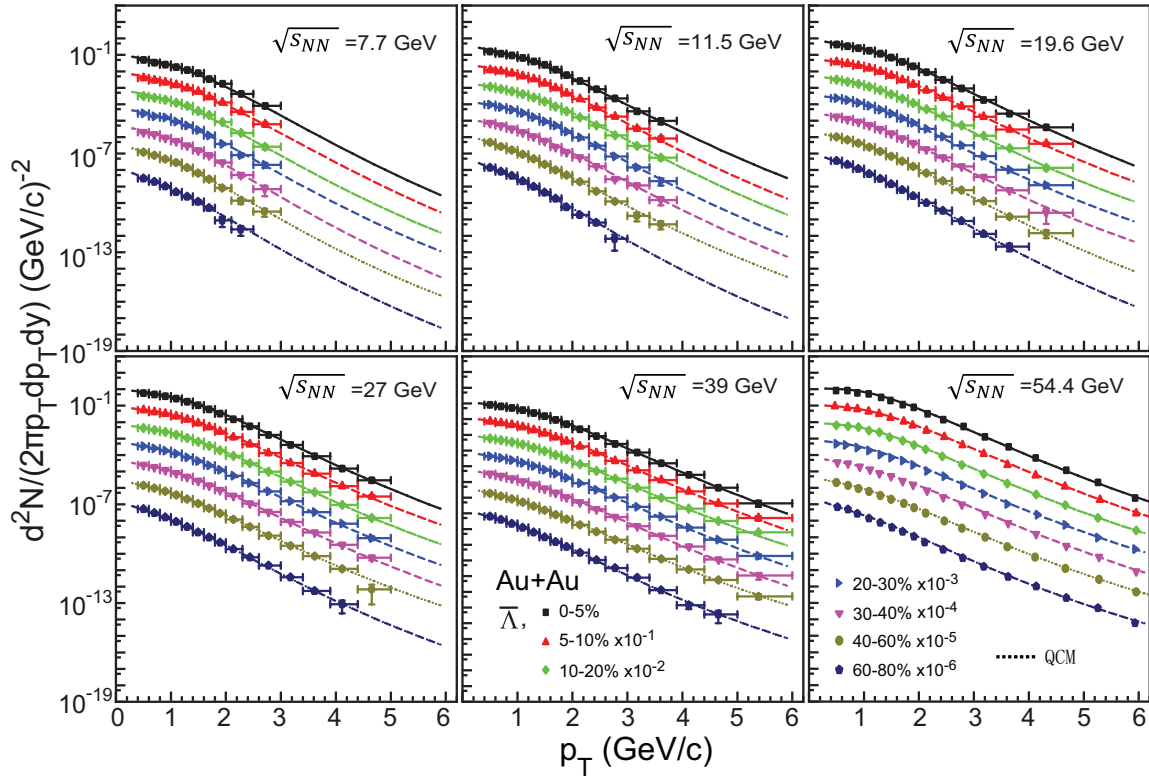
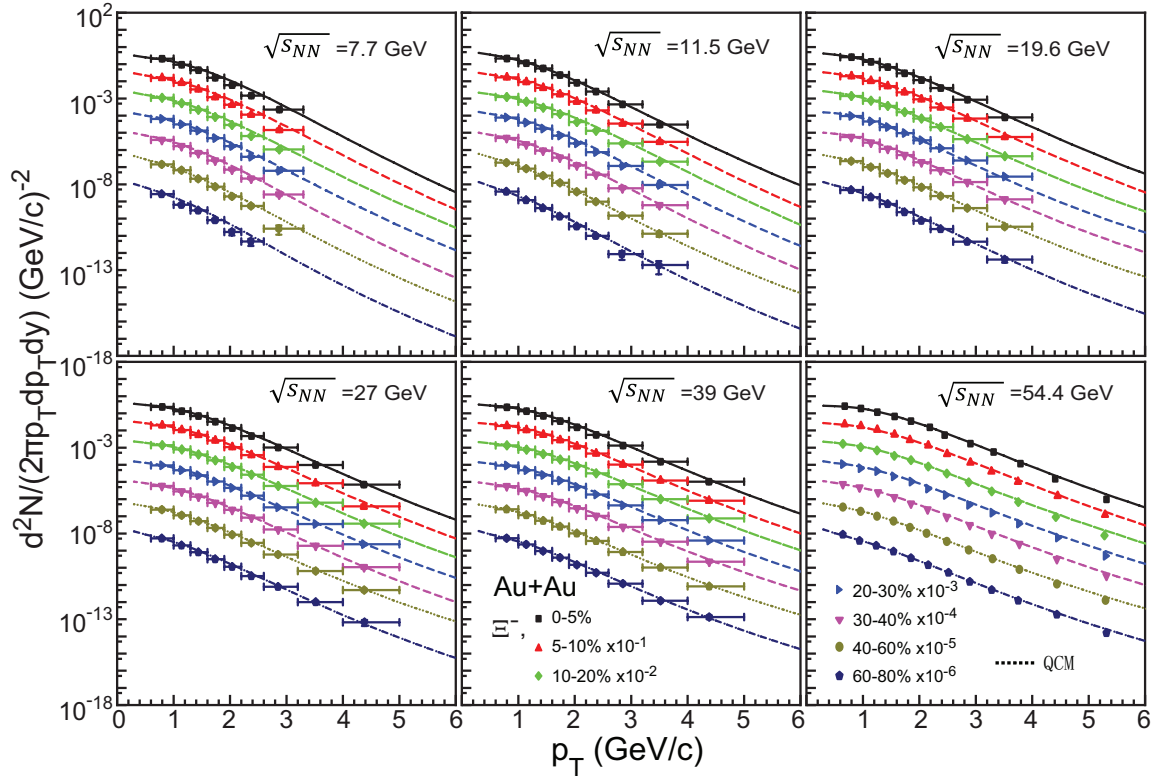
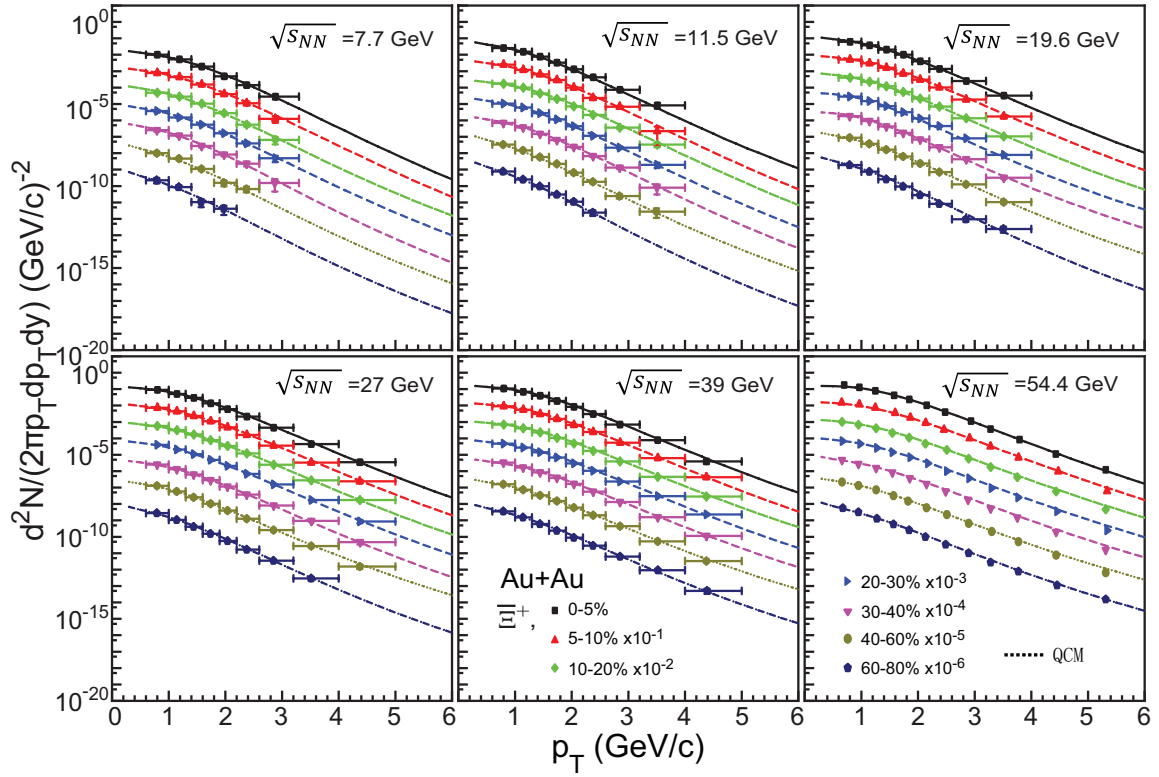
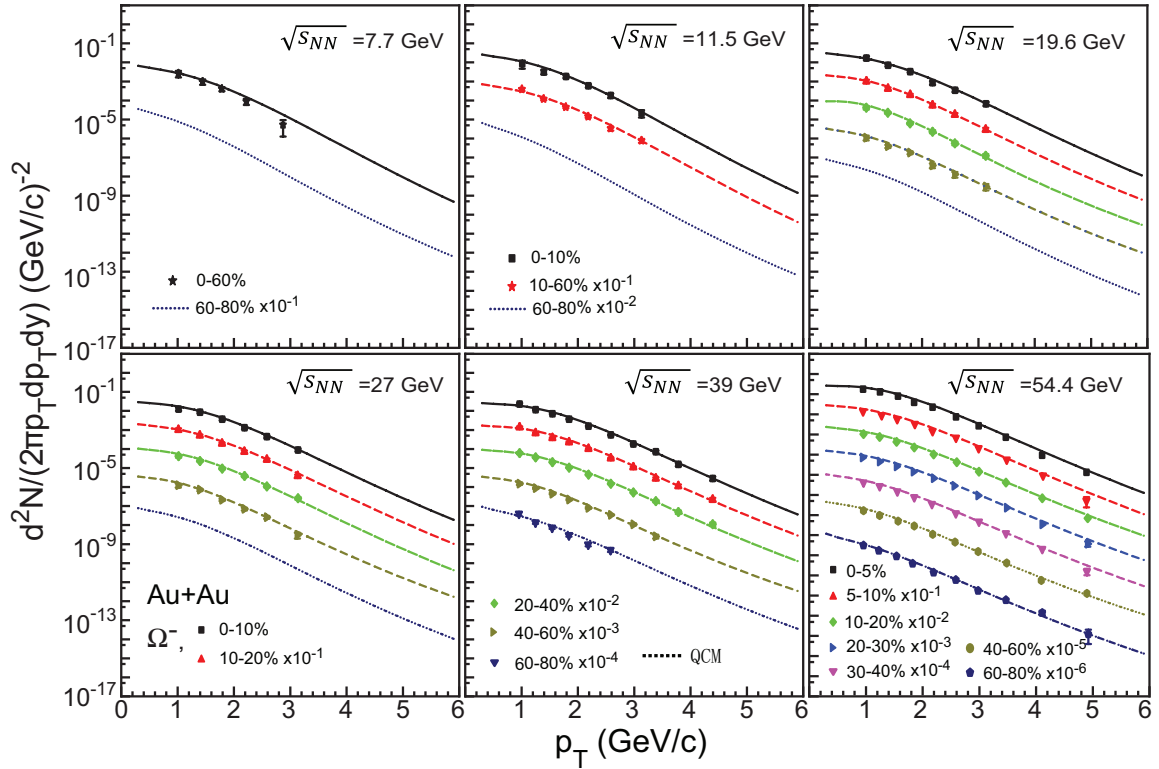
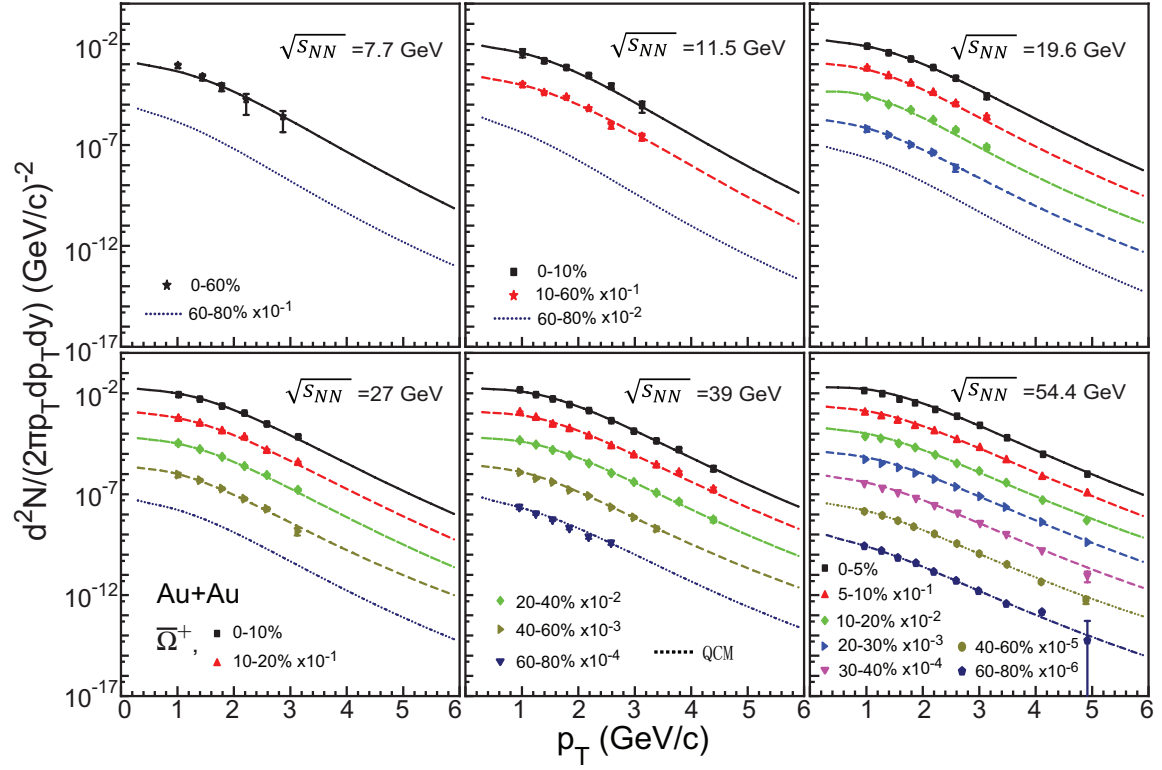
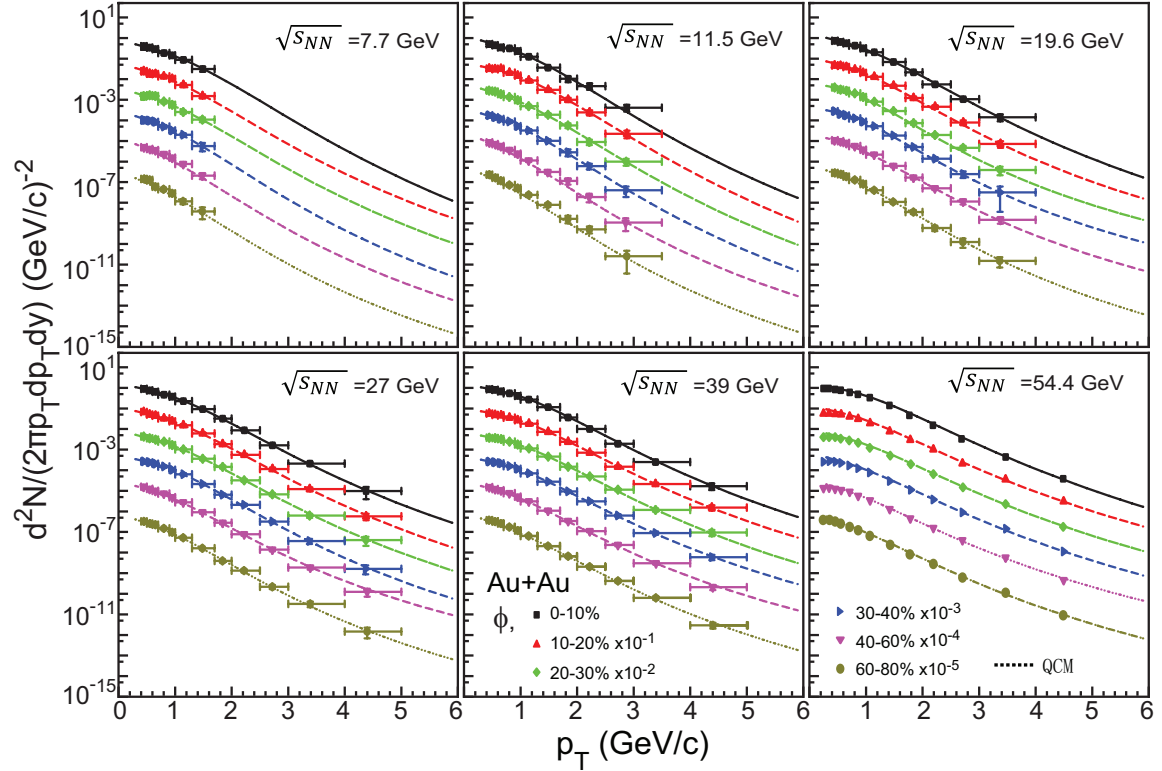


Figure 5. The same as Fig. 4 but for Λ .

Figure 6. The same as Fig. 4 but for $\bar{\Lambda}$.Figure 7. The same as Fig. 4 but for Ξ^- .

Figure 8. The same as Fig. 4 but for Ξ^+ .Figure 9. The same as Fig. 4 but for Ω^- . Experimental data are from [8, 38].

Figure 10. The same as Fig. 9 but for $\bar{\Omega}^+$.Figure 11. The same as Fig. 9 but for ϕ .

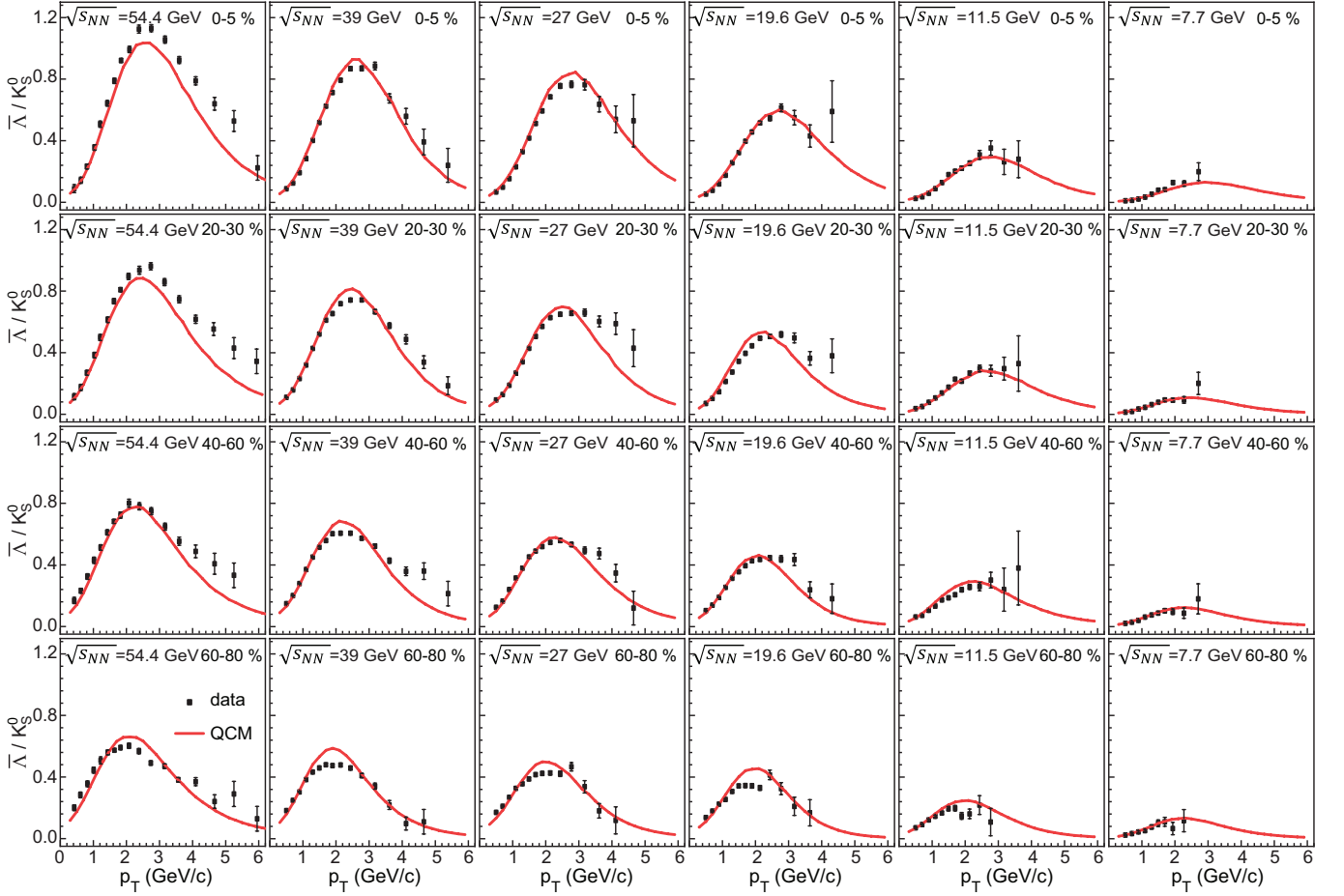


Figure 12. $\bar{\Lambda}/K_S^0$ ratio as a function of p_T at mid-rapidity ($|y| < 0.5$) for various collision centralities in Au + Au collisions at $\sqrt{s_{NN}}=7.7$ -54.4 GeV. Symbols are experimental data [7, 37] and lines are results of our model.

mainly determined by $p_T^{\alpha_u}$, which is a rapidly increasing function.

In the range $p_{T,q} \gtrsim 1$ GeV/c, quark p_T spectrum behaves approximately as

$$dN_{q_i}/dp_T \propto \left(1 + \frac{p_T}{a_i}\right)^{-n_i}, \quad (29)$$

where the stretch parameter $a_i > 0$ and indices parameter $n_i > 0$. In the studied collision energies and centralities, a is about 1-5 and n_i is about 6-20. $\bar{\Lambda}/K_S^0$ ratio in the range ($p_T \gtrsim 3$ GeV/c)

$$\begin{aligned} \frac{\Lambda}{K_S^0} &= \frac{\kappa_\Lambda f_u(x_u p_T) f_d(x_d p_T) f_s(x_s p_T)}{\kappa_K f_s(x'_s p_T) f_{\bar{u}}(x'_u p_T)} \\ &\propto (a_u + x_u p_T)^{-n_u} \\ &\times \left(1 + \frac{\Delta x_u p_T}{a_u + x_u p_T}\right)^{n_u} \left(1 + \frac{\Delta x_s p_T}{a_s + x_s p_T}\right)^{n_s}, \end{aligned} \quad (30)$$

where $\Delta x_u = x'_u - x_u = 0.1$ with $x_u = 0.45$ and $\Delta x_s = x'_s - x_s = 0.17$ with $x_s = 0.63$. Clearly, $(a_u + x_u p_T)^{-n_u}$ is the dominant term to drive Λ/K_S^0 ratio decrease with p_T

and terms $\left(1 + \frac{\Delta x_u p_T}{a_u + x_u p_T}\right)^{n_u}$ and $\left(1 + \frac{\Delta x_s p_T}{a_s + x_s p_T}\right)^{n_s}$ only weaken the influence of the first term to a certain. Combining the effect of property of quark p_T spectra in the low p_T range in Eq. (28) and that in the p_T range in Eq. (30), we now can understand the increase of Λ/K_S^0 in the range $p_T \lesssim 3$ GeV/c and subsequently its decrease in the range $p_T \gtrsim 3$ GeV/c.

Secondly, we explain that the energy dependence of the $\bar{\Lambda}/K_S^0$ ratio shown in Fig. 12, see the model calculation and experimental data in a row. There are two main physical ingredients that influence the $\bar{\Lambda}/K_S^0$ ratio. The first is the relatively rapid increase of baryon chemical potential with the decrease of collision energy. In our model, an asymmetry factor of quark-antiquark number is defined as

$$z = \frac{N_q - N_{\bar{q}}}{N_q + N_{\bar{q}}}, \quad (31)$$

which closely relates to baryon chemical potential. z causes the production asymmetry between particles and antiparticles in our model [34]. At intermediate and low RHIC energies, z is positive and is about $z \gtrsim 0.1$. This will suppress the production of anti-baryons. Therefore,

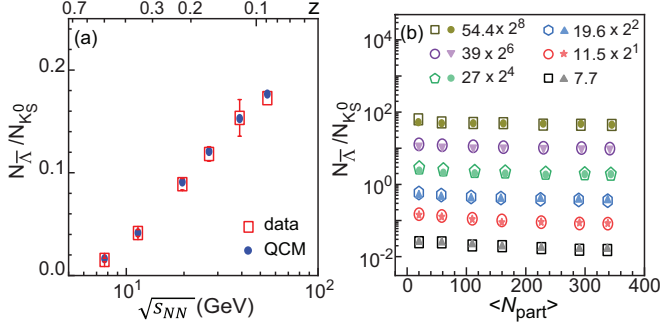


Figure 13. (a) The collision energy dependence of $N_{\bar{\Lambda}}/N_{K_S^0}$ ratios at mid-rapidity ($|y| < 0.5$) in central Au + Au collisions at $\sqrt{s_{NN}}=7.7$ -54.4 GeV. The upper horizontal axis show z of quarks; (b) $N_{\bar{\Lambda}}/N_{K_S^0}$ as functions of $\langle N_{part} \rangle$ from Au+Au collisions at $\sqrt{s_{NN}}=7.7$ -54.4 GeV. Open symbols are experimental data [7, 37] and solid symbols are model results .

the yield of $\bar{\Lambda}$ is largely suppressed and this the main reason for the decrease of $\bar{\Lambda}/K_S^0$ with the decrease of collision energy shown in Fig. 12. To illustrate it, we calculate the yield ratio of $\bar{\Lambda}$ to K_S^0 and after considering the resonance decays we obtain

$$\frac{N_{\bar{\Lambda}}}{N_{K_S^0}} = \frac{7.74}{(2 + \lambda_s)(1 + 0.12\lambda_s)} R_{\bar{B}/M}(z), \quad (32)$$

where

$$R_{\bar{B}/M}(z) = \frac{2z}{3(1+z) \left[\left(\frac{1+z}{1-z} \right)^{a-1} - 1 \right]}, \quad (33)$$

with $a \approx 4.86 \pm 0.1$ leading to $R_{\bar{B}/M}(z) \approx \frac{1}{11} - \frac{1}{12}$ in high energy collisions [34, 35]. According to the quark p_T spectra in Figs. 1-3, we can calculate z in at different collision energies and the results of $\bar{\Lambda}/K_S^0$ yield ratio are shown in Fig. 13(a) and compared with experimental data [7, 37]. We see that it decrease rapidly with the decrease of collision energy (i.e., the increase of z). This is the main reason for the globally rapid decrease of $\bar{\Lambda}/K_S^0$ ratio as the function of p_T shown in Fig. 12. Another reason that influences the behavior of $\bar{\Lambda}/K_S^0$ ratio as the function of p_T is the shape change of quark p_T spectra, which might not be clearly seen from Figs. 1-3. Actually, the extended p_T range of thermal behavior of quark p_T spectra in Eq. 27 shrink with the decrease of collision energy. This will also weaken the increasing trend of $\bar{\Lambda}/K_S^0$ ratio in the low p_T range.

Thirdly, we understand the centrality dependence of $\bar{\Lambda}/K_S^0$ ratio shown in Fig. 12, see the calculation results and experimental data in a column. As shown in Fig. 13(b), the $\bar{\Lambda}/K_S^0$ yield ratio changes weakly with collision centrality at the studied collision energies. Therefore, the weak change of z contributes small centrality dependence to $\bar{\Lambda}/K_S^0$ ratio as the function of p_T . Actually, the main influence ingredient comes from the change of quark p_T spectra at different collision centralities. From Figs. 1-3, we see a clear shrink of thermal component for

quark p_T spectra in peripheral collisions. This will cause the increase of $\bar{\Lambda}/K_S^0$ ratio in the low p_T range stops at smaller p_T in peripheral collisions than that in central collisions. The maximum value of $\bar{\Lambda}/K_S^0$ ratio can reach in peripheral collisions also smaller than that in central collisions.

Fig. 14 show Ω/ϕ ratio as the function of p_T in Au+Au collisions. Here, Ω denotes $\Omega^- + \bar{\Omega}^+$. Symbols are experimental data [8, 9, 38] and lines are model results. We see that our model results are generally in good agreement with the experimental data.

The underlying physics for the non-monotonic p_T dependence of Ω/ϕ ratio in our model is quite similar with that discussed in above $\bar{\Lambda}/K_S^0$ ratio. The difference in property between quark p_T spectra in the small p_T range $p_T \lesssim 1$ GeV/c and that in range $p_T \gtrsim 1$ GeV/c leads to the Ω/ϕ ratio firstly increases with p_T and then decrease with p_T . Because the production of Ω and ϕ involves only strange (anti-)quarks, p_T dependence of Ω/ϕ ratio can be seen more clear by the slope of the ratio

$$\left[\ln \frac{f_{\Omega}(p_T)}{f_{\phi}(p_T)} \right]' = -\frac{1}{6} p_T [\ln f_s(\xi)]'', \quad (34)$$

with $p_T/3 < \xi < p_T/2$, which is obtained in our recent work [27]. This equation means that the second derivative of the logarithm of strange quark spectrum determine the increase or decrease of the Ω/ϕ ratio. In Fig. 3 with logarithmic vertical coordinate, we can intuitively see the sign of $[\ln f_s(\xi)]''$ is negative in the range $p_{T,s} \lesssim 1$ GeV/c and is positive as $p_{T,s} \gtrsim 1$ GeV/c, which directly causes the increase of Ω/ϕ ratio in the range $p_T < 2 - 3$ GeV/c and the decrease of the ratio as p_T further increases.

The collision energy dependence of Ω/ϕ ratio in Fig. 14, see results and data in a row, is not strong. This is mainly because the Ω/ϕ yield ratio, as shown in Fig. 15(a), change weakly at the studied collision energies. The centrality dependence of Ω/ϕ ratio in Fig. 14, see results and data in a column, is relatively obvious. This is mainly because of the shape change of strange quark spectrum in different collision centralities. From Fig. 3, we see a clear shrink of thermal component for strange quark p_T spectra in peripheral collisions. This leads to the relatively weak increase of the Ω/ϕ ratio in the low p_T range and the relatively smaller p_T at which Ω/ϕ ratio begins to decrease in the peripheral collisions. The centrality dependence of Ω/ϕ yield ratio is shown in Fig. 15(b). We see that Ω/ϕ yield ratio in central collisions is larger than that in peripheral collisions to a certain extent. This is because of the increase of strange quarks fraction λ_s in central collisions. This will cause the global increase of Ω/ϕ as the function of p_T in central collisions, in comparison with the Ω/ϕ ratio in peripheral collisions.

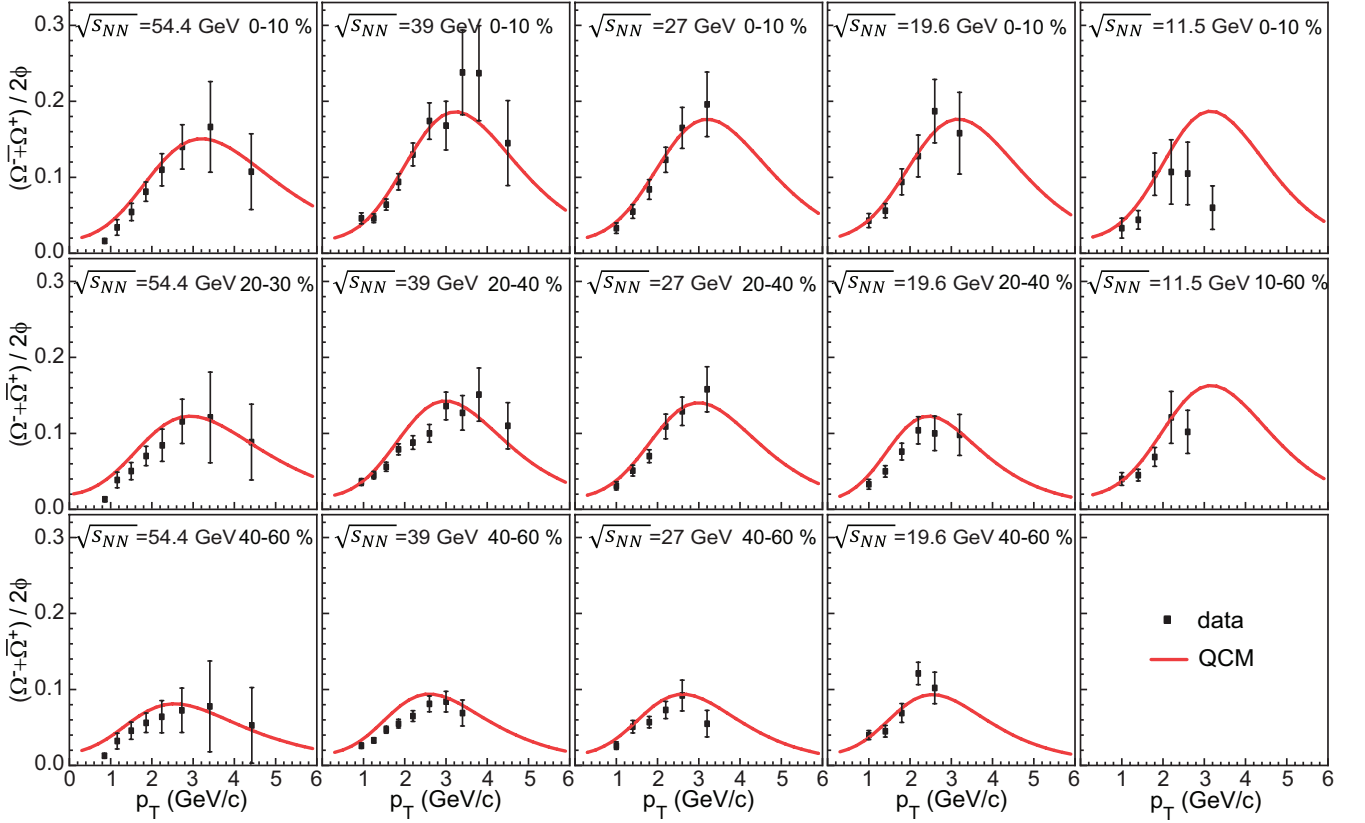


Figure 14. Ω/ϕ ratio as a function of p_T at mid-rapidity ($|y| < 0.5$) for various collision centralities in Au + Au collisions at $\sqrt{s_{NN}}=11.5$ -54.4 GeV. Symbols are experimental data [8, 9, 38] and lines are results of our model.

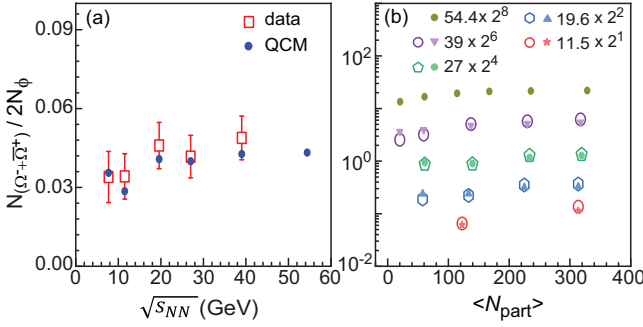


Figure 15. (a) The collision energy dependence of $N_{\Omega^-+\bar{\Omega}^-}/2N_\phi$ ratios at mid-rapidity ($|y| < 0.5$) in Au + Au collisions at $\sqrt{s_{NN}}=7.7$ -54.4 GeV; (b) $N_{\Omega^-+\bar{\Omega}^-}/2N_\phi$ as functions of $\langle N_{part} \rangle$ from Au+Au collisions at $\sqrt{s_{NN}}=11.5$ -54.4 GeV. Open symbols are experimental data [8, 9, 38] and solid symbols are model results.

V. NUCLEAR MODIFICATION FACTOR R_{CP}

The nuclear modification factor (R_{CP}) of the final hadrons is an important physical observable to quantify

the difference between hadron production in central collisions and that in peripheral collisions. R_{CP} is defined as

$$R_{CP}(p_T) = \frac{[(dN^2/2\pi p_T dp_T) / (N_{coll})]_{central}}{[(dN^2/2\pi p_T dp_T) / (N_{coll})]_{peripheral}}. \quad (35)$$

Here N_{coll} is the number of binary nucleon-nucleon collisions determined from Glauber model [40]. In general, R_{CP} of hadrons in relativistic heavy-ion collisions has a p_T dependence. The property of R_{CP} at high p_T is driven by jet quenching physics. In this paper, we focus on the property of R_{CP} of hadrons in the low and intermediate p_T range, i.e., $p_T \lesssim 4$ GeV/c for mesons and $p_T \lesssim 6$ GeV/c for baryons. The formation of hadrons in this range in our EVC mechanism is by the combination of soft quarks and antiquarks with low transverse momenta $p_{T,q} \lesssim 2$ GeV/c.

Because p_T spectra of hadrons in EVC mechanism exhibit relatively simple relationship with those of quarks and antiquarks at hadronization, R_{CP} of hadrons can also exhibit some interesting properties relating to quark flavor composition of hadron. Substituting Eq. (7) into Eq. (35), we obtain

$$\begin{aligned}
R_{CP,B_j}(p_T) &= \frac{\frac{1}{N_{coll}^{(c)}} f_{B_j}^{(c)}(p_T)}{\frac{1}{N_{coll}^{(p)}} f_{B_j}^{(p)}(p_T)} \\
&= \frac{\frac{1}{N_{coll}^{(c)}} \kappa_{B_j}^{(c)} f_{q_1}^{(c)}(x_{q_1} p_T) f_{q_2}^{(c)}(x_{q_2} p_T) f_{q_3}^{(c)}(x_{q_3} p_T)}{\frac{1}{N_{coll}^{(p)}} \kappa_{B_j}^{(p)} f_{q_1}^{(p)}(x_{q_1} p_T) f_{q_2}^{(p)}(x_{q_2} p_T) f_{q_3}^{(p)}(x_{q_3} p_T)} \\
&= \left(\frac{N_{coll}^{(c)}}{N_{coll}^{(p)}} \right)^2 \frac{\frac{N_B^{(c)}}{N_q^{(c)3}} A_{B_j}^{(c)} \left(\frac{1}{N_{coll}^{(c)}} \right)^3 f_{q_1}^{(c)}(x_{q_1} p_T) f_{q_2}^{(c)}(x_{q_2} p_T) f_{q_3}^{(c)}(x_{q_3} p_T)}{\frac{N_B^{(p)}}{N_q^{(p)3}} A_{B_j}^{(p)} \left(\frac{1}{N_{coll}^{(p)}} \right)^3 f_{q_1}^{(p)}(x_{q_1} p_T) f_{q_2}^{(p)}(x_{q_2} p_T) f_{q_3}^{(p)}(x_{q_3} p_T)} \\
&= \left(\frac{N_{coll}^{(c)}}{N_{coll}^{(p)}} \right)^2 \frac{\frac{N_B^{(c)}}{N_q^{(c)3}} A_{B_j}^{(c)}}{\frac{N_B^{(p)}}{N_q^{(p)3}} A_{B_j}^{(p)}} R_{CP,q_1}(x_{q_1} p_T) R_{CP,q_2}(x_{q_2} p_T) R_{CP,q_3}(x_{q_3} p_T). \tag{36}
\end{aligned}$$

In the third line, we have used Eq. (17). In the last line, we extend Eq. (35) to quarks at hadronization. By rewriting

$$\frac{N_B}{N_q} = \frac{2}{1+z} \frac{z}{3} \frac{(1+z)^a}{(1+z)^a - (1-z)^a} = g_B(z), \tag{37}$$

we finally obtain

$$\begin{aligned}
R_{CP,B_j}(p_T) &= \frac{A_{B_j}^{(c)} g_B(z_c)}{A_{B_j}^{(p)} g_B(z_p)} \left(\frac{N_{coll}^{(c)}/N_q^{(c)}}{N_{coll}^{(p)}/N_q^{(p)}} \right)^2 \\
&\times R_{CP,q_1}(x_{q_1} p_T) R_{CP,q_2}(x_{q_2} p_T) R_{CP,q_3}(x_{q_3} p_T). \tag{38}
\end{aligned}$$

We see that R_{CP} of baryons directly relates to the product of those of quarks. $g_B(z_c)/g_B(z_p)$ is only slightly smaller than one because z_c in central collisions is slightly greater than z_p in peripheral collisions. Coefficient $A_{B_j}^{(c)}/A_{B_j}^{(p)}$ is slightly smaller than one because quark p_T spectra become steeper to a certain extent when collision impact factor becomes large. Coefficient $\left(\frac{N_{coll}^{(c)}/N_q^{(c)}}{N_{coll}^{(p)}/N_q^{(p)}} \right)^2$ is slightly greater than one because $N_{coll} \propto N_{part}^{4/3}$ in Glauber model [40] and $N_q \propto N_{part}$ in our model. Therefore, coefficients in right hand side of Eq. (38) is about one and the product of R_{CP} of quarks dominates R_{CP} of baryons.

Applying Eq. (38) to Ω , we have

$$R_{CP,\Omega}(p_T) = \frac{A_{\Omega}^{(c)} g_B(z_c)}{A_{\Omega}^{(p)} g_B(z_p)} \left(\frac{N_{coll}^{(c)}/N_q^{(c)}}{N_{coll}^{(p)}/N_q^{(p)}} \right)^2 R_{CP,s}^3 \left(\frac{p_T}{3} \right). \tag{39}$$

A similar derivation for ϕ meson gives

$$R_{CP,\phi}(p_T) = \frac{A_{\phi}^{(c)} g_M(z_c)}{A_{\phi}^{(p)} g_M(z_p)} \left(\frac{N_{coll}^{(c)}/N_q^{(c)}}{N_{coll}^{(p)}/N_q^{(p)}} \right) R_{CP,s}^2 \left(\frac{p_T}{2} \right), \tag{40}$$

where $g_M(z) = \frac{1}{1-z} \left[1 - z \frac{(1+z)^a + (1-z)^a}{(1+z)^a - (1-z)^a} \right]$.

Fig. 16 show R_{CP} of Ω and ϕ between centrality 0 – 10% and centrality 40 – 60%. Symbols are experimental data [8, 9, 38] and lines are model results which are directly calculated from the numerical results of p_T spectra of Ω and ϕ in Figs. 9-11. We see that model results in Au+Au collisions at $\sqrt{s_{NN}} = 19.6, 27, 39$ and 54.4 GeV are in good agreement with experimental data.

Applying Eqs. (39) and (40), we can naturally explain the different p_T dependence of experimental data for R_{CP} of Ω^- and ϕ . As shown by Eqs. (39) and (40), $R_{CP,\Omega}(p_T)$ and $R_{CP,\phi}(p_T)$ in the EVC mechanism relate to the third and second power of $R_{CP,s}(p_T)$. Now, we examine the behavior of strange quark $R_{CP,s}(p_T)$, which can be calculated with Eq. (35) by strange quark p_T spectra in Fig. 17 and the results are shown in Fig. 17. We see that $R_{CP,s}(p_T)$ increases with p_T in the range $0 < p_T \lesssim 1$ GeV/c and turns to decrease with p_T in the range $p_T \gtrsim 1$ GeV/c. Because $p_{T,\phi} = 2p_{T,s}$, $R_{CP,\phi}(p_T)$ should increase with p_T in the range $p_T \lesssim 2$ GeV/c and then turns to decrease with p_T as $p_T \gtrsim 2$ GeV/c. Because $p_{T,\Omega} = 3p_{T,s}$, $R_{CP,\Omega}(p_T)$ should increase with p_T in the range $p_T \lesssim 3$ GeV/c and turns to decrease with p_T as $p_T \gtrsim 3$ GeV. Moreover, because $R_{CP,\Omega}(p_T)$ relates to the third power of $R_{CP,s}(p_T)$ but $R_{CP,\phi}(p_T)$ relates to the square of $R_{CP,s}(p_T)$, $R_{CP,\Omega}(p_T)$ can not only keep the increase trend in the larger p_T range but also reach higher magnitude, which are just seen in experimental data.

In view of this good agreement and simple expressions

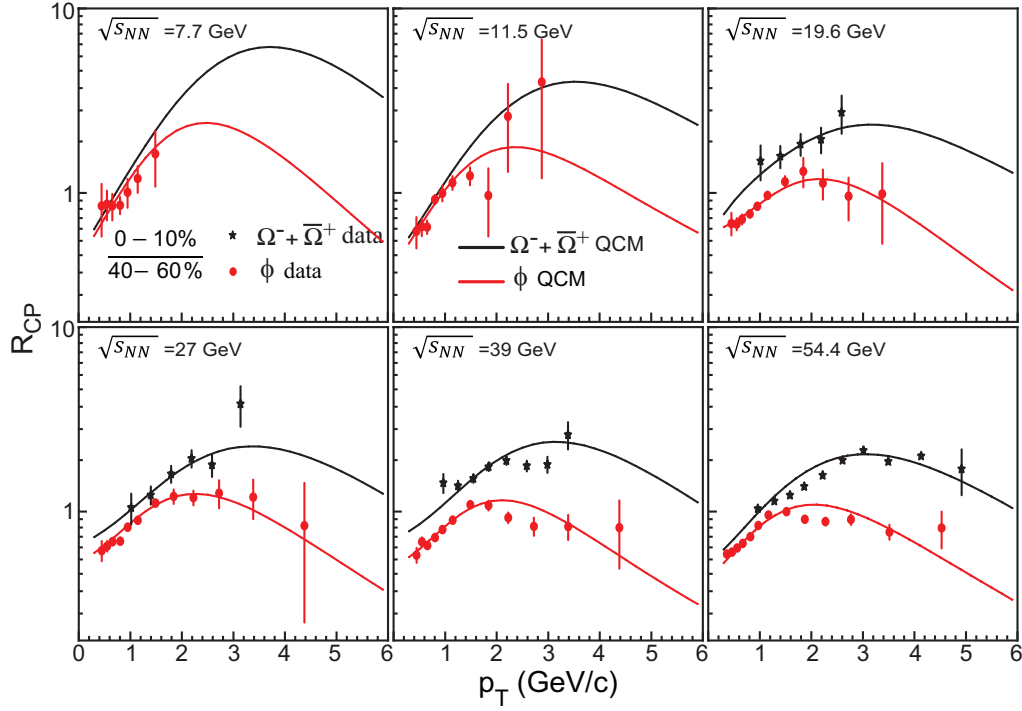


Figure 16. $R_{CP}(0-10\%)/(40-60\%)$ of $\Omega^- + \bar{\Omega}^+$, ϕ , at mid-rapidity ($|y| < 0.5$) in Au+Au collisions at $\sqrt{s_{NN}}=7.7-54.4$ GeV. Symbols are experimental data [8, 9, 38] and lines are results of our model.

for Ω^- and ϕ in Eqs. (39) and (40), we can further build a correlation

$$R_{CP,\Omega}^{1/3}(3p_T) = M_q R_{CP,\phi}^{1/2}(2p_T), \quad (41)$$

where

$$M_q = \frac{A_\Omega^{(c)\frac{1}{3}} A_\phi^{(p)\frac{1}{2}} g_B^{\frac{1}{3}}(z_c) g_M^{\frac{1}{2}}(z_p)}{A_\Omega^{(p)\frac{1}{3}} A_\phi^{(c)\frac{1}{2}} g_B^{\frac{1}{3}}(z_p) g_M^{\frac{1}{2}}(z_c)} \left(\frac{N_{coll}^{(c)}/N_q^{(c)}}{N_{coll}^{(p)}/N_q^{(p)}} \right)^{\frac{1}{6}} \quad (42)$$

is close to one. Fig. 18 show the results of Eq. (41) for experimental data of Ω and ϕ . The coefficient M_q is 1.16, 1.15, 1.18 at three collisional energies, respectively. The deviation of the M_q from 1 is due to the influence of three parts. Numerical calculations give the $(A_\Omega^{(c)\frac{1}{3}} A_\phi^{(p)\frac{1}{2}})/(A_\Omega^{(p)\frac{1}{3}} A_\phi^{(c)\frac{1}{2}})$ is 1.03, 1.02, 1.06, the $(g_B^{\frac{1}{3}}(z_c) g_M^{\frac{1}{2}}(z_p))/(g_B^{\frac{1}{3}}(z_p) g_M^{\frac{1}{2}}(z_c))$ is 1.05, 1.04, 1.01, and the $(N_{coll}^{(c)}/N_q^{(c)})^{\frac{1}{6}}/(N_{coll}^{(p)}/N_q^{(p)})^{\frac{1}{6}}$ is 1.07, 1.08, 1.10, respectively.

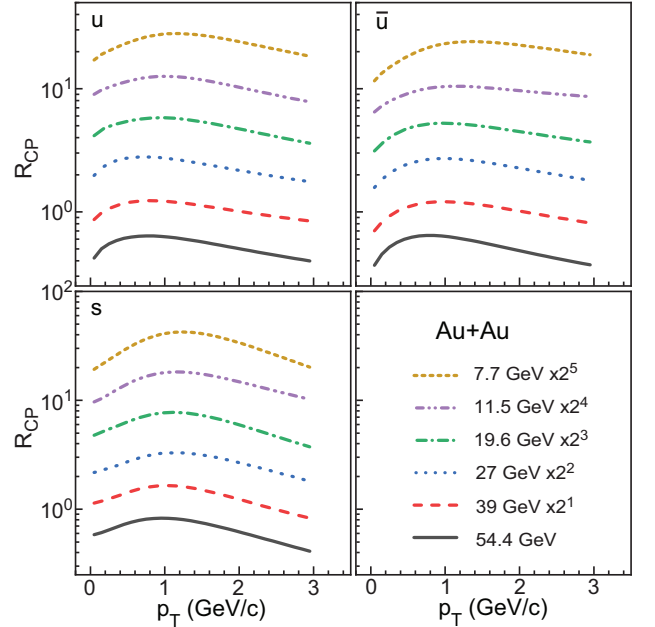


Figure 17. $R_{CP}(0-5\%)/(40-60\%)$ of u , \bar{u} and $R_{CP}(0-10\%)/(40-60\%)$ of s at mid-rapidity ($|y| < 0.5$) in Au+Au collisions at $\sqrt{s_{NN}}=7.7-54.4$ GeV.

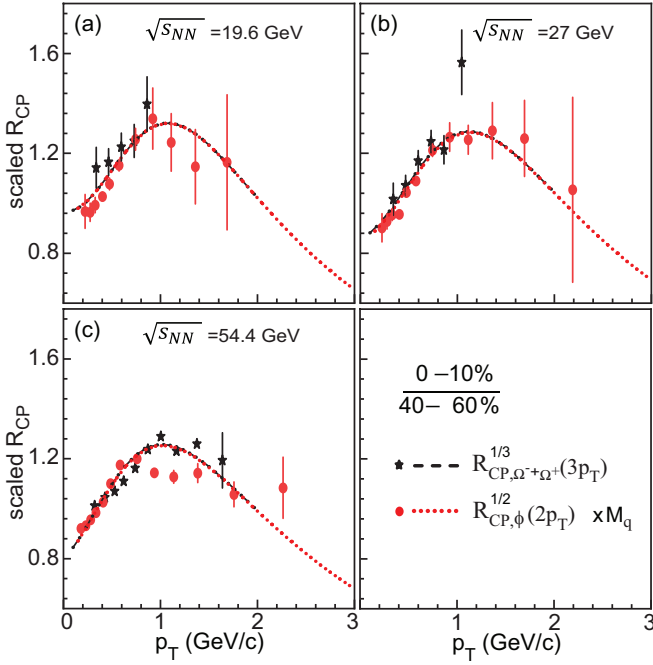


Figure 18. The scaling property for $R_{CP}(0-10\%)/(40-60\%)$ of $\Omega^- + \bar{\Omega}^+$ and ϕ at mid-rapidity ($|y| < 0.5$) in Au+Au collisions at $\sqrt{s_{NN}}=7.7-54.4$ GeV. Symbols are experimental data [8, 9, 38] and lines are results of our model. The coefficient M_q is 1.16, 1.15 and 1.18, respectively.

R_{CP} of K_S^0 , Λ and Ξ in the EVC mechanism are

$$R_{CP,\Lambda}(p_T) \quad (43)$$

$$= \frac{A_{\Lambda}^{(c)} g_B(z_c)}{A_{\Lambda}^{(p)} g_B(z_p)} \left(\frac{N_{coll}^{(c)}/N_q^{(c)}}{N_{coll}^{(p)}/N_q^{(p)}} \right)^2 R_{CP,u}^2(x_u p_T) R_{CP,s}^2(x_s p_T),$$

$$R_{CP,\Xi}(p_T) \quad (44)$$

$$= \frac{A_{\Xi}^{(c)} g_B(z_c)}{A_{\Xi}^{(p)} g_B(z_p)} \left(\frac{N_{coll}^{(c)}/N_q^{(c)}}{N_{coll}^{(p)}/N_q^{(p)}} \right)^2 R_{CP,u}(x_u p_T) R_{CP,s}^2(x_s p_T),$$

$$R_{CP,K}(p_T) \quad (45)$$

$$= \frac{A_K^{(c)} g_M(z_c)}{A_K^{(p)} g_M(z_p)} \left(\frac{N_{coll}^{(c)}/N_q^{(c)}}{N_{coll}^{(p)}/N_q^{(p)}} \right) R_{CP,u}(x_u p_T) R_{CP,s}(x_s p_T),$$

R_{CP} of these hadrons not only depend on the R_{CP} of strange quarks but also depend on that of up/down quarks.

Fig. 19 shows R_{CP} of Λ , Ξ and K_S^0 in Au+Au collisions at six collisional energies. Symbols are experimental data [7, 37]. Lines of different kinds are our model results which are calculated from their model results of inclusive p_T spectra shown in Figs. 4-8. We see that the experimental data of three hadrons exhibit some hierarchy properties. Compared with R_{CP} of Λ and Ξ , R_{CP} of K_S^0 at $\sqrt{s_{NN}} = 19.6 - 54.4$ GeV reach the maximum at

a smaller p_T (i.e., $p_T \approx 1.5 - 2$ GeV/c) and is lower than those of Λ and Ξ as $p_T \gtrsim 2$ GeV/c. R_{CP} of Λ is smaller in magnitude than that of Ξ to a certain extent but is quite similar with the latter in the global p_T dependence. Our model reproduce these hierarchy properties. The last few points of R_{CP} for K_S^0 at $\sqrt{s_{NN}} = 7.7$ and 11.5 GeV in range $p_T \gtrsim 2$ GeV/c are close to those of baryons, which is beyond the model expectation.

Using Eqs. (43)-(45) and R_{CP} of quarks shown in Fig. 18, we can naturally explain the experimental data of R_{CP} of Λ , Ξ and K_S^0 . We see that R_{CP} of u , \bar{u} and s are all dependent on p_T . R_{CP} of (anti-)quark increases with p_T at low p_T and turns to decrease with p_T as $p_T \gtrsim 1$ GeV/c. R_{CP} of K_S^0 relates to the product of two quark R_{CP} , and therefore R_{CP} of K_S^0 reaches the maximum at $p_T \approx 2$ GeV/c. R_{CP} of Λ and Ξ relate to the product of three quark R_{CP} , therefore they reaches the maximum at $p_T \approx 3$ GeV/c and the maximum values are higher than that of K_S^0 . This is quite similar to the case of Ω and ϕ discussed above. We also see from Fig. 18 that R_{CP} of strange quarks has a stronger non-monotonic p_T dependence than that of u and \bar{u} . In addition, because the fraction of strange quarks (i.e., $\lambda_s = N_s/N_{\bar{u}}$) in central collisions is higher than that in peripheral collisions, R_{CP} of strange quarks is globally higher than that of u or \bar{u} to a certain extent. Since Ξ has two strange quarks, R_{CP} of Ξ has a stronger p_T dependence than that of Λ and is globally higher than that of Λ .

VI. SUMMARY

In this paper, we have applied an equal-velocity quark combination to systematically study p_T spectra of strange hadrons K_S^0 , ϕ , Λ , Ξ^- , Ω^- , $\bar{\Lambda}$, $\bar{\Xi}^+$ and $\bar{\Omega}^+$ at mid-rapidity in Au+Au collisions at $\sqrt{s_{NN}} = 7.7, 11.5, 19.6, 27, 39$ and 54.4 GeV. The model was proposed in [22, 29] by inspiration of the quark number scaling property of hadronic p_T spectra in pp and pPb collisions at LHC energies and has a series of successful applications in describing hadron production in pp and pPb collisions at LHC as well as AA collisions at both RHIC and LHC [20, 23-28]. Application of this model to STAR BES energies can further test the universal property of the hadronization in different collisions. In the study, we focus on the self-consistent explanation on p_T spectra of strange hadrons at STAR BES energies. Therefore we not only carried out the global comparison with p_T spectra data of these hadrons but also concentrated on baryon-to-meson ratios and nuclear modification factor in the low and intermediate p_T range which are sensitive to hadronization mechanism.

We firstly carried out a global fit to experimental data of p_T spectra of strange hadrons. The model has three quark inputs, i.e., $f_u(p_T)$, $f_{\bar{u}}(p_T)$ and $f_s(p_T)$. We used the data of Λ , $\bar{\Lambda}$ and ϕ to fix them and subsequently calculated p_T spectra of K_S^0 , Ξ^- , Ω^- , $\bar{\Xi}^+$, $\bar{\Omega}^+$ and compared them with experimental data. We evaluated the

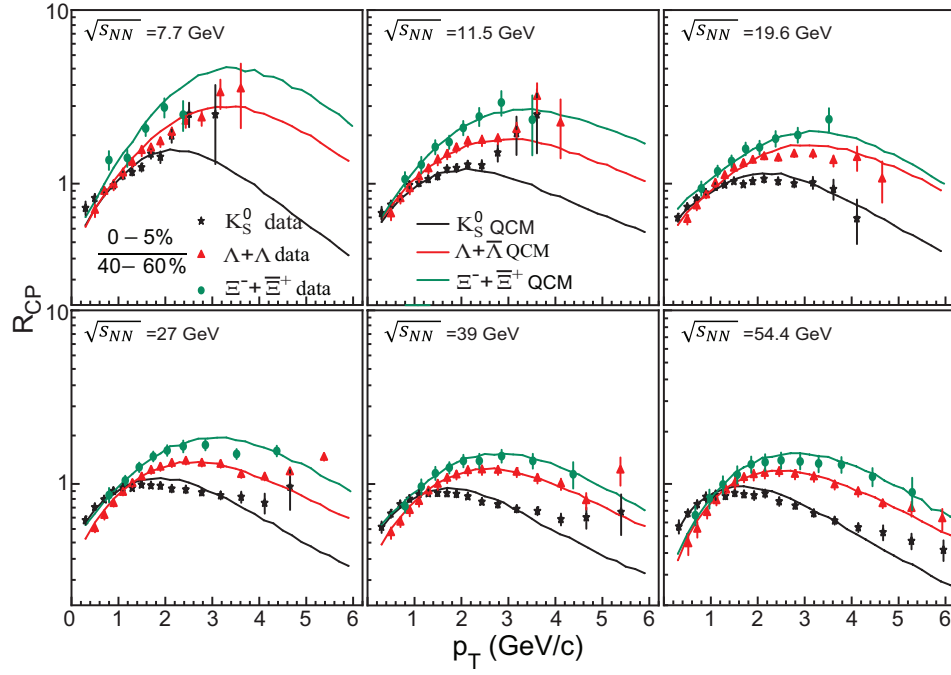


Figure 19. R_{CP} of K_S^0 , $\Lambda + \bar{\Lambda}$ and $\Xi^- + \bar{\Xi}^+$ (0-5%)/(40-60%) at mid-rapidity ($|y| < 0.5$) in Au+Au collisions at $\sqrt{s_{NN}}=7.7$ -54.4 GeV. Symbols are experimental data [7, 37] and lines are results of our model.

relative deviation between model calculation and experimental data of these eight hadrons. We found that the relative deviation is generally about 2-3% at $\sqrt{s_{NN}} = 27, 39, 54.4$ GeV and in central collisions at 7.7, 11.5, 19.6 GeV. The deviation slightly increases up to about 4% in semi-central and peripheral collision at $\sqrt{s_{NN}} = 7.7, 11.5, 19.6$ GeV. These results indicate that our model can give a globally consistent explanation on p_T spectra of these strange hadrons at the studied collision energies.

We studied the dependence of two baryon-to-meson ratios $\bar{\Lambda}/K_S^0$ and Ω/ϕ on p_T , collision centrality and collision energy. By classifying the property of quark p_T spectra in the range $p_T \lesssim 1$ GeV/c and that in the range $p_T \gtrsim 1$ GeV/c, we provided an intuitive explanation on the increase of two ratios in the range $p_T \lesssim 2 - 3$ GeV/c and their subsequent decrease at larger p_T . Combining the extracted quark p_T spectra at hadronization, we further discussed the quark level origin of the change of global magnitude and the movement of peak position of two ratios in different collision centrality and at different collision energies.

We studied the nuclear modification factor R_{CP} of strange hadrons. Taking advantage of the analytic fea-

ture of EVC mechanism, we derived the analytic expression for R_{CP} of hadrons and found that R_{CP} of hadrons can be written as the product of those of quarks at hadronization besides some p_T -independent coefficients. Using these analytic formulas, we gave an intuitive explanation on the difference between R_{CP} of meson and that of baryon, including the difference in peak position and peak value of the R_{CP} . In addition, the hadron species dependence of R_{CP} of Λ, Ξ, Ω can be also naturally understood by considering the property of R_{CP} of quarks at hadronization.

VII. ACKNOWLEDGMENTS

This work is supported in part by the National Natural Science Foundation of China under Grant No. 11975011 and 12175115, Shandong Provincial Natural Science Foundation (Grant No. ZR2019YQ06, ZR2019MA053), and Higher Educational Youth Innovation Science and Technology Program of Shandong Province (Grant No. 2019KJJ010).

-
- [1] J. Rafelski and B. Muller, *Phys. Rev. Lett.* **48**, 1066 (1982), *Phys.Rev.Lett.* 56, 2334 (1986).
 [2] B. I. Abelev *et al.* (STAR), *Phys. Rev. C* **77**, 044908 (2008), [arXiv:0705.2511 \[nucl-ex\]](https://arxiv.org/abs/0705.2511).
 [3] B. Abelev *et al.* (ALICE), *Phys. Lett. B* **728**, 216 (2014), [Erratum: *Phys.Lett.B* 734, 409–410 (2014)], [arXiv:1307.5543 \[nucl-ex\]](https://arxiv.org/abs/1307.5543).

- [4] C. Alt *et al.* (NA49), *Phys. Rev. C* **78**, 034918 (2008), [arXiv:0804.3770 \[nucl-ex\]](#).
- [5] J. Adam *et al.* (STAR), *Phys. Rev. C* **102**, 034909 (2020), [arXiv:1906.03732 \[nucl-ex\]](#).
- [6] L. Adamczyk *et al.* (STAR), *Phys. Rev. C* **93**, 021903 (2016), [arXiv:1506.07605 \[nucl-ex\]](#).
- [7] M. U. Ashraf (STAR), *28th International Conference on Ultrarelativistic Nucleus-Nucleus Collisions*, (2019).
- [8] Y. Huang (STAR), *19th International Conference on Strangeness in Quark Matter*, (2021).
- [9] Y. Huang (STAR), *EPJ Web Conf.* **259**, 03002 (2022).
- [10] F. A. Flor, G. Olinger, and R. Bellwied, *Phys. Lett. B* **814**, 136098 (2021), [arXiv:2009.14781 \[nucl-ex\]](#).
- [11] J. Chen, J. Deng, Z. Tang, Z. Xu, and L. Yi, *Phys. Rev. C* **104**, 034901 (2021), [arXiv:2012.02986 \[nucl-th\]](#).
- [12] L.-L. Li, F.-H. Liu, M. Waqas, and M. Ajaz, *Universe* **8**, 31 (2022), [arXiv:2201.02069 \[hep-ph\]](#).
- [13] M. Waqas, F.-H. Liu, R.-Q. Wang, and I. Siddique, *Eur. Phys. J. A* **56**, 188 (2020), [arXiv:2007.00825 \[hep-ph\]](#).
- [14] V. Greco, C. M. Ko, and P. Lévai, *Phys. Rev. C* **68**, 034904 (2003), [arXiv:nucl-th/0305024](#).
- [15] R. J. Fries, B. Müller, C. Nonaka, and S. A. Bass, *Phys. Rev. Lett.* **90**, 202303 (2003), [arXiv:nucl-th/0301087 \[nucl-th\]](#).
- [16] D. Molnar and S. A. Voloshin, *Phys. Rev. Lett.* **91**, 092301 (2003), [arXiv:nucl-th/0302014](#).
- [17] R. C. Hwa and C. B. Yang, *Phys. Rev. C* **67**, 034902 (2003), [arXiv:nucl-th/0211010 \[nucl-th\]](#).
- [18] L.-W. Chen and C. M. Ko, *Phys. Rev. C* **73**, 044903 (2006), [arXiv:nucl-th/0602025 \[nucl-th\]](#).
- [19] X.-H. Jin, J.-H. Chen, Y.-G. Ma, S. Zhang, C.-J. Zhang, and C. Zhong, *Nucl. Sci. Tech.* **29**, 54 (2018).
- [20] J. Song, X.-F. Wang, H.-H. Li, R.-Q. Wang, and F.-L. Shao, *Phys. Rev. C* **103**, 034907 (2021), [arXiv:2007.14588 \[nucl-th\]](#).
- [21] Y. J. Ye, J. H. Chen, Y. G. Ma, S. Zhang, and C. Zhong, *Chin. Phys. C* **41**, 084101 (2017), [arXiv:1706.00894 \[nucl-th\]](#).
- [22] J. Song, X.-r. Gou, F.-l. Shao, and Z.-T. Liang, *Phys. Lett. B* **774**, 516 (2017), [arXiv:1707.03949 \[hep-ph\]](#).
- [23] J. Song, H.-h. Li, and F.-l. Shao, *Eur. Phys. J. C* **78**, 344 (2018), [arXiv:1801.09402 \[hep-ph\]](#).
- [24] H.-H. Li, F.-L. Shao, J. Song, and R.-Q. Wang, *Phys. Rev. C* **97**, 064915 (2018), [arXiv:1712.08921 \[hep-ph\]](#).
- [25] J.-w. Zhang, H.-h. Li, F.-l. Shao, and J. Song, *Chin. Phys. C* **44**, 014101 (2020), [arXiv:1811.00975 \[hep-ph\]](#).
- [26] J. Song, F.-l. Shao, and Z.-t. Liang, *Phys. Rev. C* **102**, 014911 (2020), [arXiv:1911.01152 \[nucl-th\]](#).
- [27] H.-H. Li, F.-L. Shao, and J. Song, (2021), [arXiv:2103.14900 \[hep-ph\]](#).
- [28] R.-Q. Wang, J. Song, F.-L. Shao, and Z.-T. Liang, *Phys. Rev. C* **101**, 054903 (2020), [arXiv:1911.00823 \[hep-ph\]](#).
- [29] X.-r. Gou, F.-l. Shao, R.-q. Wang, H.-h. Li, and J. Song, *Phys. Rev. D* **96**, 094010 (2017), [arXiv:1707.06906 \[hep-ph\]](#).
- [30] J. Song, H.-h. Li, and F.-l. Shao, *Eur. Phys. J. C* **81**, 1 (2021), [arXiv:2008.03017 \[nucl-th\]](#).
- [31] J. Adam *et al.* (ALICE), *Eur. Phys. J. C* **76**, 245 (2016), [arXiv:1601.07868 \[nucl-ex\]](#).
- [32] S. Acharya *et al.* (ALICE), *Phys. Lett. B* **807**, 135501 (2020), [arXiv:1910.14397 \[nucl-ex\]](#).
- [33] D. Adamova *et al.* (ALICE), *Eur. Phys. J. C* **77**, 389 (2017), [arXiv:1701.07797 \[nucl-ex\]](#).
- [34] J. Song and F.-l. Shao, *Phys. Rev. C* **88**, 027901 (2013), [arXiv:1303.1231 \[nucl-th\]](#).
- [35] F.-l. Shao, G.-j. Wang, R.-q. Wang, H.-h. Li, and J. Song, *Phys. Rev. C* **95**, 064911 (2017), [arXiv:1703.05862 \[hep-ph\]](#).
- [36] K. Olive, K. Agashe, and C. Amsler (Particle Data Group), *Chin. Phys. C* **38**, 090001 (2014).
- [37] J. Adam *et al.* (STAR), *Phys. Rev. C* **102**, 034909 (2020), [arXiv:1906.03732 \[nucl-ex\]](#).
- [38] L. Adamczyk *et al.* (STAR), *Phys. Rev. C* **93**, 021903 (2016), [arXiv:1506.07605 \[nucl-ex\]](#).
- [39] L. Adamczyk *et al.* (STAR), *Phys. Rev. C* **96**, 044904 (2017), [arXiv:1701.07065 \[nucl-ex\]](#).
- [40] M. L. Miller, K. Reygers, S. J. Sanders, and P. Steinberg, *Ann. Rev. Nucl. Part. Sci.* **57**, 205 (2007), [arXiv:nucl-ex/0701025](#).